HHS Public Access

Author manuscript

Dev Cell. Author manuscript; available in PMC 2018 August 07.

Published in final edited form as:

Dev Cell. 2017 August 07; 42(3): 286–300.e4. doi:10.1016/j.devcel.2017.07.010.

Primary Cilia Signaling Shapes the Development of Interneuronal Connectivity

Jiami Guo[1,2], **James M. Otis**[1,3], **Holden Higginbotham**[1,2], **Chase Monckton**[1], **Gang Cheng Jr**[1], **Aravind Asokan**[4], **Kirk Mykytyn**[5], **Tamara Caspary**[6], **Garret D. Stuber**[1,3], and **E. S. Anton**[1,2,^]

[1]UNC Neuroscience Center, University of North Carolina School of Medicine, Chapel Hill, NC 27599

[2]Department of Cell Biology and Physiology, University of North Carolina School of Medicine, Chapel Hill, NC 27599

[3]Department of Psychiatry, University of North Carolina School of Medicine, Chapel Hill, NC 27599

[4]Department of Genetics and Gene Therapy Center, University of North Carolina School of Medicine, Chapel Hill, NC 27599

[5]Department of Biological Chemistry and Pharmacology, Neuroscience Research Institute, The Ohio State University, OH 43210

[6]Department of Human Genetics, Emory University School of Medicine, Atlanta, GA 30322

Summary

Appropriate growth and synaptic integration of GABAergic inhibitory interneurons are essential for functional neural circuits in the brain. Here, we demonstrate that disruption of primary cilia function following the selective loss of ciliary GTPase Arl13b in interneurons impairs interneuronal morphology and synaptic connectivity, leading to altered excitatory/inhibitory activity (E/I) balance. The altered morphology and connectivity of cilia mutant interneurons and the functional deficits are rescued by either chemogenetic activation of ciliary GPCR signaling or the selective induction of Sstr3, a ciliary-GPCR, in Arl13b deficient cilia. Our results thus define a specific requirement for primary cilia-mediated GPCR signaling in interneuronal connectivity and inhibitory circuit formation.

eTOC Blurb

[^]Correspondence to: E. S. Anton, UNC Neuroscience Center and the Department of Cell Biology and Physiology, The University of North Carolina School of Medicine, Chapel Hill, NC 27599, anton@med.unc.edu, PHONE: 919-843-6114 FAX: 919-966-1844.
Lead Contact: E. S. Anton

Author contributions

J.G., H.H., J.O., A.A, K.M., T.C, G.S., and E.A. designed the experiments and supervised the project. J.G., J.O., and H.H. conducted the experiments and analyzed the data. J.G., H.H., J.O., G.S., and E.A. wrote the manuscript.

Growth and connectivity of interneurons are fundamental to the formation of functional neural circuitry. Guo et al. show that primary cilia signaling, via Arl13b-GPCR pathway, promotes interneuronal connectivity and inhibitory circuit formation. Primary cilia signaling is a non-synaptic signaling mechanism through which environmental signals can shape and refine interneuronal networks.

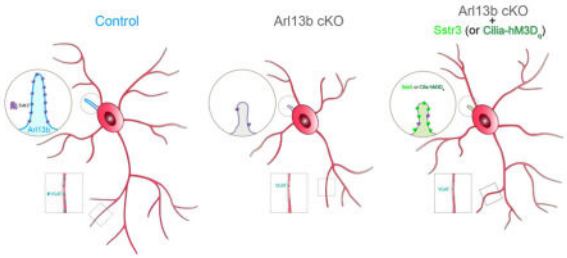

Keywords

Primary cilia; interneurons; circuitry; GPCR signaling; Joubert syndrome related disorders; autism spectrum disorders

Introduction

Appropriate connectivity and integration of GABAergic interneurons (INs) are essential for the formation of functional neuronal circuitry in the brain. Disrupted IN circuit formation, homeostasis and the resultant excitatory/inhibitory (E/I) imbalance is a convergent mechanism underlying neurodevelopmental disorders such as autism spectrum disorders (ASD), schizophrenia, and intellectual disabilities (Bourgeron, 2009; Kepecs and Fishell, 2014; Marín, 2012). INs, originating from the ventral telencephalon, migrate widely in different trajectories to populate distinct brain regions and integrate into local neural circuits (Guo and Anton, 2014; Marín, 2013; Touzot et al., 2016). Extensive efforts have been made toward understanding the fate specification and migration of INs (Kepecs and Fishell, 2014; Marín, 2013). However, the developmental mechanisms that regulate the assembly of INs into functional circuits are not well understood. Local environment, through synaptic or non-synaptic mechanisms are thought to exert profound influence over the formation and architecture of IN circuits (Betley et al., 2009; Close et al., 2012b; De Marco García et al., 2011; De Marco García et al., 2015; Kepecs and Fishell, 2014; Pieraut et al., 2014). Here, we tested whether primary cilium, an essential sensor of environmental cues and a signal transduction hub, plays a determinant role in the environmental modulation of IN morphology and connectivity necessary for circuit assembly (Guemez-Gamboa et al., 2014).

Primary cilia contain signal transduction components necessary to transmit efficient intracellular responses to extracellular stimuli. The critical role of primary cilia in brain development and function is evident in human ciliopathies (Guemez-Gamboa et al., 2014; Guo et al., 2015), where disrupted cilia function lead to brain malformations and behavioral deficits. Many candidate genes for neurodevelopmental disorders such as ASD, schizophrenia, and intellectual disabilities affect cilia function (Hildebrandt et al., 2011; Lee and Gleeson, 2011; Louvi and Grove, 2011; Marley and Von Zastrow, 2012). Therapeutic

drugs such as lithium used in the treatment of neurobehavioral disorders can modulate cilia mediated chemosensory functions in neurons(Miyoshi et al., 2009). Further, neuronal cilia are enriched in signaling machinery such as neurotransmitter receptors, GPCRs, ion channels, and Ca^{2+} and thus have been hypothesized to non-synaptically modulate neuronal function (Green and Mykytyn, 2014). The association of cilia dysfunction with neurodevelopmental disorders and the specialized signaling abilities of cilia raise the intriguing possibility that impaired cilia function during brain development and the resultant changes in neural circuitry may contribute to the emergence of intellectual disabilities and enhance the sensitivity for neuropsychiatric disorders (NPDs) such as ASD.

We therefore examined how disrupted primary cilia signaling affects the formation and function of striatal interneuronal circuitry, dysfunction of which is widely implicated in the pathophysiology of a spectrum of NPDs (Clark et al., 2009; Shepherd, 2013). The striatum integrates glutamatergic inputs from the cortex and thalamus and send GABAergic, inhibitory projections to neurons in the basal ganglia (Evans et al., 2012; Gittis and Kreitzer, 2012). To assess the specific requirement of interneuronal primary cilia signaling in the construction of inhibitory circuit, we conditionally disrupted primary cilia function in the striatal INs originating from the medial ganglionic eminence (MGE). Arl13b, a small GTPase of the Arf/Arl family, is specifically localized to cilia and is required for cilium's ability to function as a signaling hub (Cantagrel et al., 2008b; Caspary et al., 2007; Guo et al., 2015; Higginbotham et al., 2012b; Higginbotham et al., 2013). Deletion of Arl13b impairs primary ciliary signal transduction, without physically ablating ciliary structure, and thus provides a unique model for examining the specific role of primary cilia signaling in interneuronal morphology, connectivity, and synaptic integration. Our results demonstrate that the disruption of cilia function perturbs interneuronal circuit development. Connectivity of cilia mutant striatal interneurons (INs), ciliary Ca^{2+} signaling, and ciliary localization of GPCRs such as Sstr3 are altered. Notably, deficits in the morphology and connectivity of cilia mutant INs are rescued by the cilia-selective induction of Sstr3 or chemogenetic, DREADD mediated activation of GPCR signaling in Arl13b deficient cilia. Together, these studies define a hitherto unknown role of primary cilia-GPCR signaling in striatal IN connectivity.

Results

Primary ciliary signaling is required for interneuronal morphology

To assess the functional significance of primary cilia in the emergence of IN morphology and connectivity, we selectively inactivated *Arl13b* in the developing INs. Nkx2.1-Cre line, which expresses Cre in medial ganglionic eminence (MGE) and preoptic area, was crossed with a floxed allele of *Arl13b* (Xu et al., 2008). MGE gives rise to the majority of GABAergic Parvalbumin$^+$ (PV^+) and somatostatin$^+$ (SST^+) INs in the striatum. Nkx2.1Cre thus enables specific interneuron targeting and does not affect striatal medium spiny neuron (MSN) population. A Cre reporter *Lox-STOP-Lox-Ai3* allele was incorporated to label INs with YFP. Arl13b is absent in the primary cilia of Cre^+/YFP^+ INs (Figure S1A–D) in *Nkx2.1Cre; Arl13b$^{Lox/lox}$; Ai3* (*Nkx-Arl13b; Ai3*) mice. Deletion of *Arl13b* in MGE did not adversely affect the production or survival of INs (Data not shown).

We first assessed the consequences of Arl13b deletion on interneuronal morphological development. At P30, when the morphological maturation of INs is largely complete (Chattopadhyaya et al., 2004), immunolabeling of the PV^+ and SST^+ INs revealed significantly reduced dendritic and axonal complexity throughout the striatum (Figure 1A–D). Similar changes were also evident in PV^+ INs in cortex and hippocampus (Figure S2A–D). To further quantify the changes in interneuronal dendritic and axonal processes, newborn *Nkx-Arl13b; Ai3* mice and control littermates were injected with Cre inducible AAV2-CAG-FLEX-tdTomato virus to sparsely label Cre^+ INs. Reconstruction of labeled INs at P30 revealed significantly reduced axonal length, axonal branching, as well as dendritic complexity in mutant PV^+ (Figure 1E, F, I) and SST^+ INs (Figure 1G, H, J). Together, these results suggest that deletion of Arl13b in interneuronal cilia leads to striatal IN morphological defects.

Nkx2.1-Cre is active in INs from the time of birth. To examine if primary ciliary signaling regulates interneuron morphological development, independently of their potential function in early IN development, we generated *Parv-Cre; Arl13b$^{Lox/lox}$; Ai9 (Parv-Arl13b; Ai9)* mice, in which Cre is expressed in PV^+ INs from around postnatal week two, after the completion of IN generation and placement (Korotkova et al., 2010; Dehorter et al, 2015) (Figure S3A–B). At P30, cortical interneuron morphology was not affected in *Parv-Arl13b* cortex (Higginbotham et al, 2012). However, by P60 in *Parv-Arl13b; Ai9* mice, a significant reduction in PV^+ interneuronal process complexity in the striatum (Figure 1K, L), cortex, and hippocampus (Figure S3C–F) was evident without associated changes in the PV^+ cell density. PV^+ neurite density ($tdTom^+$) was reduced by 45.5 ± 2.2% in *Parv-Arl13b; Ai9* mice compared to controls (Figure 1K, L). Together, these analyses of Arl13b deletion in INs at different developmental stages indicate a specific requirement for primary ciliary signaling in the morphological development of striatal INs.

Primary ciliary signaling is required for IN synaptic connection

The morphological defects observed in Arl13b deficient PV^+ and SST^+ INs prompted us to examine their synaptic connections. Since PV^+ INs preferentially form perisomatic synapses, we examined the density of YFP^+ boutons of PV^+ INs around the soma of $NeuN^+$ medium spiny neurons (MSNs) in control and Arl13b deficient striatum. Compared to controls, PV^+ perisomatic boutons were significantly reduced in both density and size in *Nkx-Arl13b; Ai3* INs (Figure 2A–D). Similarly, the density and size of $tdTomato^+$ or $VGAT^+$ perisomatic boutons were also reduced in *Parv-Arl13b; Ai9* (Figure 2E–L) striatum. We also observed a similar reduction in the average density of perisomatic boutons in the cortex of *Nkx-Arl13b* (Figure S2E–H) and *Parv-Arl13b* (Figure S3G–J) mice compared to controls. Further, to analyze synaptic boutons of single IN axons at high resolution, we imaged virally (AAV2-CAG-FLEX-tdTomato) labeled PV^+ and SST^+ INs in control and *Nkx-Arl13b* mice. Arl13b deficient axons of INs displayed reduced synaptic bouton density and size (Figure 2M–T). A similar reduction in the average density of $VGAT^+$ presynaptic boutons along the axons of Arl13b deficient INs is also evident *in vitro* (Figure S4). Together, these results demonstrate that ciliary Arl13b deletion disrupts synaptic connectivity of INs.

Functional impact of impaired primary cilia signaling in interneurons

To assess the electrophysiological consequences of impaired primary cilia signaling and IN morphology on interneuronal synaptic activity, we performed patch-clamp recordings in the dorsal striatum of brain slices from control and *Nkx-Arl13b; Ai9* mice. Miniature inhibitory and excitatory postsynaptic currents (mIPSCs and mEPSCs) were sampled from MSNs. Compared to control littermates, recordings from MSNs of *Nkx-Arl13b; Ai9* mice revealed a decrease in mIPSC frequency in cilia mutant mice (Figure 3A, B). In contrast, no changes in mIPSC amplitude (Figure 3C), mEPSC frequency (Figure 3D, E), or mEPSC amplitude (Figure 3D, F) were found in MSNs of *Nkx-Arl13b; Ai9* mice. The specific decrease in the inhibitory synaptic input onto projecting MSNs of cilia mutant mice, leads to excitatory/inhibitory synaptic imbalance (Figure 3G). Thus, consistent with the cellular characterization of IN synaptic connectivity, these electrophysiological data confirm a functional deficit in the synaptic activities of cilia mutant INs.

Primary ciliary GPCR signaling activity is required for interneuron connectivity

To define the ciliary signaling mechanisms underlying the disrupted connectivity of INs, we analyzed changes in primary cilia signaling characteristics in Arl13b deficient INs. Calcium signaling is a hallmark of ciliary signaling activity (Belgacem and Borodinsky, 2011; DeCaen et al., 2013; Su et al., 2013). We therefore examined cilia-specific calcium dynamics in Arl13b deficient INs using a genetically encoded single fluorescence calcium indicator (GECO1.0) targeted selectively to primary cilia (Cilia-GECO1.0) (Su et al., 2013). ATP is known to trigger an increase in ciliary calcium level that normally proceeds through primary cilia from the base to tip (Su et al., 2013). ATP stimulation of *Nkx-Arl13b* INs showed a 63 ± 8.2% reduction in Ca^{2+} elevation compared to controls (Figure 4A–C).

In wt mouse embryonic fibroblasts (MEFs), Cilia-GECO1.0 displayed a uniform activity along the whole primary cilia (Figure 4D–E). However, Ca^{2+} activity in mutant cilia is preferentially detected in the basal area (Figure 4F, arrow) with weaker activity throughout the rest of the cilium (Figure 4F), suggesting a deficiency in ciliary Ca^{2+} signal transduction. Upon ATP stimulation, Ca^{2+} spike in wt cells appeared first at base and subsequently traveled towards the tip of the cilium (Figure 4D). In contrast, mutant cilia showed a 55±4.7% and 77±3.6% reduction in Ca^{2+} elevation at cilia base and tip, respectively (Figure 4D, F, H–K).

To further characterize the ciliary, calcium dynamics of INs, we electroporated Cilia-GECO1.0 plasmids into the GE of control and *Nkx-Arl13b; Ai9* embryos (E15.5) and imaged interneuronal ciliary calcium dynamics in brain slices prepared at P0. Primary cilia in control neurons display Ca^{2+} “hot spots” that show changes in intensity (Figure 4L, arrowheads and arrow). These Ca^{2+} “hot spots” periodically emerge, travel, and disappear within control primary cilia, indicating dynamic signal transduction activities. In contrast, Arl13b deficient cilia are characterized by the lack of such dynamic Ca^{2+} intensity changes or “hot spot” activity (Figure 4M, N). Together, these observations suggest that Arl13b deletion lead to primary cilia signal transduction defects in INs.

Calcium dynamics in cilia is a hallmark of ciliary G-protein-coupled receptor (GPCR) signaling activity (Cantagrel et al., 2008b; Caspary et al., 2007). Considering the pivotal role of GPCR signaling in the formation, function, and plasticity of neural circuits, we first asked if the ciliary expression of somatostatin receptor 3 (Sstr3), a GPCR known to be highly enriched throughout neuronal cilia and crucial for striatal functions (Green et al., 2012), is disrupted in Arl13b deficient INs. Sstr3 is aberrantly distributed in *Nkx-Arl13b* cilia and compared to control, only (11±9%) express it normally. Expression of wild type Arl13b, but not non ciliary Arl13b (Arl13b^{V358}) in *Nkx-Arl13b* INs rescues this defect (Arl13b: 82±12%, Arl13b^{V358}: 15±12%). Arl13b deficiency driven changes in ciliary targeting of GPCRs such as Sstr3 may underlie cilia signaling defects. We therefore asked if expression of Sstr3 in Arl13b- deficient interneuron cilia could compensate for the ciliary signal transduction deficiency and ameliorate the IN connectivity defects. We generated *Nkx2.1-Cre; Arl13b$^{Lox/lox}$; Ai9; Sstr3-GFP* (O'Connor et al., 2013) (*Nkx-Arl13b-Sstr3)* mice to test this We observed that in *Nkx-Arl13b-Sstr3* mice, in which Sstr3 expression is induced in Arl13b deficient interneurons (Figure 5A–E), Sstr3-GFP localizes to cilia and was not detected in non ciliary compartments of the INs. Arl13b deficient cilia are likely to have retained elements of mechanisms needed for ciliary localization of GPCR receptors (e.g., Tubby and Tulp3; Badgandi et al., 2016), albeit at disrupted levels. Perhaps this is what enables the localization of over expressed Sstr3-GFP to Arl13 deficient cilia in *Nkx-Arl13b-Sstr3* mice. We examined IN morphology and synaptic connectivity in *Nkx-Arl13b-Sstr3* mice as before and found that Sstr3 expressing Arl13b deficient INs exhibited similar morphology as controls (Figure 5A–C). Further, both *in vivo* and in dissociated INs, we observed a similar rescue of the synaptic bouton density and size following Sstr3 expression (Figure 5F–O; Figure S5). Importantly, patch-clamp recordings confirmed a rescue of the mIPSC frequency of MSNs and E/I imbalance in *Nkx-Arl13b-Sstr3* mice (Figure 5P–V). Further, expression of a non functional Sstr3 point mutant (D124E; Green et al., 2016) that disrupts ligand binding, but localizes to cilia, fails to rescue Arl13b deficient phenotype (Figure S5D). Thus, the expression of Sstr3, a ciliary-GPCR, in Arl13b deficient INs helped rescue the defective IN morphology and synaptic connectivity.

To further examine the function of cilia specific GPCR signaling in striatal interneuronal circuit development, we used a chemogenetic approach to gain precise spatio-temporal control of GPCR signaling in primary cilia and evaluated if activation of ciliary GPCR signaling rescues IN circuit disruption in cilia mutants. This approach entails IN cilia-specific expression of mutant GPCRs (Designer Receptors Exclusively Activated by Designer Drugs (DREADDs) that have been evolved to be activated by the pharmacologically inert small molecule clozapine N-oxide (CNO) (Armbruster et al., 2007; Dong et al., 2010). hM3D$_q$ DREADD couples to Gq and can induce Ca^{2+} activation when activated by CNO.

We generated cilia-targeted hM3D$_q$ DREADD (Cilia-hM3D$_q$) and found that Cilia-hM3D$_q$ displayed highly enriched ciliary expression in INs and MEFs (Figure 6A; Figure S6). INs were then co-transfected with cilia- targeted Cilia-hM3D$_q$ and cilia calcium indicator Cilia-RFP-GECO1.0. Upon 10μM CNO treatment, control cilia co-expressing Cilia-hM3D$_q$ and Cilia-RFP-GECO1.0 showed a 74 ± 12% increase of relative RFP intensity (Figure 6B–C).

Thus cilia targeted DREADD allow us to manipulate cilia-specific GPCR and related Ca^{2+} signaling.

To evaluate if modulation of ciliary GPCR signaling can rescue IN circuit disruption in cilia mutants, we transfected INs from *Nkx-Arl13b; Ai9* brains with Cilia-hM3D$_q$. INs were then maintained in media supplemented with CNO (10μM) or DMSO for 2 weeks. We hypothesized that activation of ciliary-GPCR signaling in the mutant INs may rescue the mutant morphology and connectivity phenotype. Consistent with our hypothesis, in Arl13b deficient INs, activation of ciliary-GPCR signaling leads to a rescue of morphology and synaptic connections (Figure 6D–H).

Human mutations in ARL13B disrupt interneuron connectivity

To date, four different mutations in ARL13B have been identified in Joubert syndrome patients (Figure 7A) (Cantagrel et al., 2008b; Thomas et al., 2015). To test whether the expression of the mutant alleles of human ARL13B affects interneuron connectivity, we generated Cre- inducible, human wild type ARL13B and human mutant AAV constructs (R79Q, W82X, Y86C, R200C) and expressed them in INs dissociated from *Nkx-Arl13b* brains. This approach enables us to selectively express human wild type or mutant ARL13B in Arl13b null INs and query the effects of human ARL13B mutations on IN morphology and connectivity. While wild-type human ARL13B rescued the morphological and synaptic defects in the Arl13b deficient INs, JSRD causing variants R79Q, W82X, Y86C failed to do so (Figure 7 B–G, J–M). Expression of JSRD causing variant R200C partially rescued the morphological, but not the synaptic connection defects in Arl13b deficient INs (Figure 7H, J–M). Together, these results demonstrate that expression of disease causing alleles of human ARL13B in INs disrupt primary ciliary signal transduction and thus interneuronal connectivity.

We further investigated whether the requirement for Arl13b in interneuron development is specifically due to its ciliary expression and activity by using a nonciliary form of Arl13b, Arl13b^{V358A}. A point mutation (V-A) at residue 358 abolishes the cilia localization of Arl13b, but retains its normal GTPase activity (Higginbotham et al., 2012). Similar to the human mutations, Arl13b^{V358A} did not rescue the developmental defects in Arl13b deficient INs (Figure 7I, J–M), suggesting that primary ciliary localization and activity of Arl13b is required for its role in the regulation of interneuronal morphology and connectivity.

Discussion

Our results show that primary cilia signaling is essential for the connectivity of striatal interneurons and disruption of this process can lead to circuit malformation in the striatum, a known contributor to the emergence of neuropsychiatric disorders. Further, these circuit malformations can be ameliorated by the ciliary activation of GPCRs in cilia mutant INs.

Earlier studies have demonstrated that primary cilia and Arl13b activities also modulate interneuronal migration in embryonic cerebral cortex (Baudoin et al., 2012; Higginbotham et al., 2012). The current analysis of postnatal interneuronal development in striatum indicate that the ciliary effect on interneuronal morphology and connectivity is distinct from the

embryonic effect and likely not a consequence of it. The density of interneurons in postnatal striatum was not affected in *Nkx-Arl13* mice (control: 17.6±2.4/10Kμm^2, *Nkx-Arl13*: 18.8±1.6/10Kμm^2) and, importantly, post migratory, interneuron- specific inactivation of Arl13b in *Parv-Arl13* mice and disrupted growth and connectivity of isolated Arl13b-deficient interneurons *in vitro* clearly demonstrate the selective effect of Arl13b in post migratory interneuronal morphology and connectivity (Figures 1, 2, and S4). Although how primary cilia modulate distinct aspects of neuronal development (i.e., neurogenesis, migration, growth, and connectivity) remains to be fully deciphered (Guo et al., 2015; Harwell et al., 2012), many known signaling pathways that regulate interneuronal migration (e.g., Erb4/Neuregulin-1; Flames et al., 2004), also exert migration- independent effects on interneuron circuitry and function (Fazzari et al., 2010).

The connectivity and synaptic integration of GABAergic interneurons are influenced by local environment (Chattopadhyaya, 2011; Chattopadhyaya et al., 2004; Chattopadhyaya et al., 2007; Maroof et al., 2013; Pieraut et al., 2014), modulated by experience and activity (Chattopadhyaya et al., 2004; Chattopadhyaya et al., 2007; Close et al., 2012a; Close et al., 2012b; De Marco García et al., 2011; Denaxa et al., 2012; Donato et al., 2013; Kinney et al., 2006; Pieraut et al., 2014). Primary cilium is a sensory organelle of environmental stimuli. Our results demonstrate that disruption of primary ciliary signaling in PV$^+$ and SST$^+$ striatal INs results in deficits in their morphology, connectivity, and function. These observations reveal a non-synaptic signaling mechanism through which environmental signals can shape and refine neuronal networks. We also observed similar defects in cilia mutant INs in cerebral cortex and hippocampus, indicating a general requirement for the primary cilia mediated signaling in the development of interneuronal morphology and connectivity.

Imbalance in E/I ratio caused by disrupted GABAergic interneuron network homeostasis has been proposed as a major converging mechanism of NPDs (Consortium et al., 2013; Consortium et al., 2015; Lee and Gleeson, 2011; Parikshak et al., 2013; Voineagu et al., 2011). The prolonged postnatal maturation and sensitivity to environmental modulation of the GABAergic networks may facilitate this common biological vulnerability. Our identification of a primary cilia-based mechanism in interneuron functional connectivity illustrates how local environment can impact circuit assembly and function through atypical avenues. A spectrum of behavioral characteristics of NPDs have been associated with human ciliopathies (Alvarez Retuerto et al., 2008; Amann-Zalcenstein et al., 2006; Lee and Gleeson, 2011; Marley and Von Zastrow, 2012; Hildebrandt et al., 2011). Many candidate genes for ASD, schizophrenia, and intellectual disabilities exert potent effects on cilia function (Hildebrandt et al., 2011; Marley et al., 2013; Marley and Von Zastrow, 2012). While increasing number of investigations have focused on causative, individual genetic variants of NPDs, the identification of common biological nodes of vulnerabilities that underlie the pathophysiology of NPDs is equally critical for the development of effective therapeutic interventions for NPDs. The association of cilia dysfunction with NPDs (Green and Mykytyn, 2014; Guo et al., 2015; Lee and Gleeson, 2011) raises the intriguing possibility that primary cilium, unique in its ability to function as an integrative sensor and conveyor of critical environmental signals during circuit formation, represents one such node of vulnerability.

How does primary cilia signaling participate in the environmental modulation of interneuron connectivity? Further, how can primary cilium, a few μm long, small organelle localized at cell soma, exert a physiological effect on the whole neuron? Our findings on interneuron ciliary Ca^{2+} dynamics and ciliary-GPCR signaling shed some light on these questions. Recent studies using genetically encoded, cilia targeted calcium indicators revealed that primary cilium is a specialized calcium signaling hub that holds a much higher resting, as well as a wider dynamic range of Ca^{2+} concentration than the cytoplasm (DeCaen et al., 2013; Delling et al., 2013; Su et al., 2013). Primary cilia are known to utilize calcium as a second messenger for triggering signaling cascades (Green and Mykytyn, 2014). We adapted this Ca^{2+} indicator tool to provide a glimpse into the dynamic calcium signaling within interneuronal cilia. The ciliary calcium dynamics in INs is likely a reflection of the signaling activities within cilia as they probe and respond to the surrounding environment. The loss of this signaling dynamics in mutants is indicative of the changes in signaling emanating from Arl13b deficient cilia.

Primary cilium is emerging as a unique cellular compartment for enriched G-protein-coupled receptor (GPCR) signaling in many cell types (Adamantidis et al., 2005; Berbari et al., 2008; Brailov et al., 2000; Brear et al., 2014; Händel et al., 1999; Hwang and Mukhopadhyay, 2015; Loktev and Jackson, 2013; Omori et al., 2015; Soetedjo et al., 2013). Studies in olfactory epithelium and photoreceptors have demonstrated that activation of ciliary GPCRs is capable of trigging signaling cascades that lead to calcium influx and ultimately the depolarization of the cell (Green and Mykytyn, 2014). Genetic and pharmacological approaches have shown that function of ciliary-GPCRs such as Sstr3, 5-HT6, MCHR1 impact cognitive functions including learning and memory, anxiety and depression, seizure activity, and feeding behaviors. Deficits in these functions are commonly associated with human ciliopathies (Adamantidis et al., 2005; Einstein et al., 2010; Qiu et al., 2008; Svenningsson et al., 2007; Hildebrandt et al., 2011; Lee and Gleeson, 2011). In this study, using chemogenetic activation of cilia-targeted DREADDs ($hM3D_q$) and induced ciliary expression of Sstr3, we show that ciliary-GPCR signaling is a key regulator of interneuronal connectivity. Shh signaling appears not to affect IN connectivity (Xu et al., 2005). Sstr3 ligand somatostatin is abundantly expressed in the brain. However, the dynamics of somatostatin and other GPCR ligands' access to cilia during IN connectivity remains to be elucidated. Additionally, Sstr3 can form heterodimers with other Sstrs, as well as with other GPCRs and receptor tyrosine kinases to generate synergistic, antagonistic or completely unique signals due to changes in G protein coupling (Einstein et al., 2010; Green et al., 2012; Viollet et al., 2008). Recent studies also indicate that normal ciliary signaling involves ectocytosis of activated GPCRs, such as Sstr3, from ciliary tips (Nager et al., 2016). The nature of such interactions in IN cilia is yet to be fully understood. Further, Sstr3 is likely to be one of the many GPCRs contributing to IN development. The expression and function of other cilia localized GPCRs (e.g., D1R, D2R, D5R, NPY2R, NPY5R, PGR15L, Gpr161, GPR19/83/88, GAL2R, GAL3R, HTR6, KISS1R, MCHR1, NPFFR1, P2RY1, PRHLR, and QRFPR) in INs remains to be characterized (Badgandi et al., 2017; Loktev and Jackoson, 2013). The lack of rescue with D124E-Sstr3 confirms the importance of cilary Sstr3 activity in INs, but other non- ciliary roles of Sstr3 in these neurons cannot be ruled out. Functional evaluation of non-cilia targeted Sstr3 in Arl13b deficient INs will help

clarify this further. Nevertheless, our findings provide an example of the impact of ciliary-GPCR signaling on inhibitory network construction and function.

Four distinct mutations (p. R79Q, p. W82X, Y86C, p. R200C) in highly conserved domains of ARL13B have been identified in JSRD patients: the R79Q substitution interferes with GTP binding, W82X introduces a stop codon in exon 3, Y86C is a missense mutation in switch II region, and R200C is a missense mutation within the C terminal, coiled-coiled domain (Cantagrel et al., 2008a; Cantagrel et al., 2008b; Miertzschke et al., 2014; Thomas et al., 2015). Three of the mutations, R79Q, W82X, and Y86C are clustered in the GTP-binding domain and are known to destabilize the structure or functional integrity of the GTP-binding domain. Our results show that the expression of R79Q, W82X, and Y86C fail to rescue the morphological and synaptic connectivity defects of Arl13b deficient INs, suggesting that these disease causing alleles may disrupt cilia functions during IN development and connectivity. Interestingly, R200C, the mutation in the coiled-coiled domain, partially rescued IN morphology, but did not affect synaptic connectivity. R200C mutation, which is known to destabilize the GTP-binding domain structure, may have disrupted Arl13b activity and there might be a differential requirement for distinct functional domains of Arl13b between IN morphological vs. synaptic connection development. Further, different ARL13B mutations may also affect the axoneme structure of cilia, in addition to disrupting downstream signaling partners such as INPP5E (Caspary et al., 2007; Cevik et al., 2010; Humbert et al., 2012) necessary for ciliary GPCR targeting. In the absence of Arl13b, the B-tubules of the 9 microtubule doublets in the axoneme are often open and not attached to the A-tubule of the doublets (Caspary et al., 2007). Anterograde intraflagellar transport trains, containing ciliary components, move along the B-tubules (Stepanek and Pigino, 2016). Disruption of this process, together with the loss of downstream effectors such as INPP5E necessary for GPCR localization, are likely to have contributed to the disrupted Sstr3 receptor localization and signaling defects in Arl13 deficient cilia. In addition to Arl13b, Tubby and Tulp3 can also regulate Sstr3 localization (Badgandi et al., 2016). Presence of some of these proteins, even at disrupted levels, in Arl13b deficient cilia, may have enabled localization of over expressed Sstr3-GFP to Arl13 deficient cilia in *Nkx-Arl13b-Sstr3* mice. Creation of Arl13b structure-function models in which ciliary structure defects and signaling receptor transport/localization defects can be clearly separated will be highly useful in fully understanding the functions of Arl13b. A structurally ‘normal’ Arl13b cilia mutant model that lacks a normal repertoire of GPCR signaling receptors will help understand the relative contributions of Arl13b to cilia structure and signaling.

In the future, it will be important to examine the possible participation of ciliary signaling in the conveyance of experience-driven environmental regulation of interneuronal connectivity and plasticity during critical period (Baraban et al., 2009; Chattopadhyaya et al., 2004; Southwell et al., 2010). Recent studies identified IGF1, a ligand for Igf1R receptors in cilia (Higginbotham et al., 2013; Lehtinen et al., 2011), as a sensory experience regulated gene necessary to sculpt the synaptic connections of vasoactive intestinal peptide (VIP) interneurons (Mardinly et al., 2016). It is also possible that ciliary signaling is continuously required in mature neurons for the modulation and maintenance of neuronal network homeostasis. Further, the source and the identity of the various environmental cues that trigger primary cilia signaling in INs and whether such signaling enables INs to function

cooperatively (Karnani et al., 2016) are yet to be fully characterized. The exact downstream signaling cascades of ciliary signaling, including ciliary-GPCR signaling, and their precise cellular and physiological effect on neuronal function during cognitive activities such as learning and memory also remain to be elucidated. Future efforts aimed at answering these questions will further our understanding of the newly identified role of primary cilia in neuronal circuit formation and function.

EXPERIMENTAL MODEL AND SUBJECT DETAILS

Mice

Mice were cared for according to the guidelines approved by the University of North Carolina. Light/dark cycle in the vivarium is 7/7 hours. Animals were housed in groups of 3 adults per cage. Arl13b null mice (*Arl13b*$^{hnn/hnn}$) were generated as described in Caspary et al., 2007 (Caspary et al., 2007). *Arl13b* was conditionally inactivated in interneurons by crossing *Arl13b*$^{Lox/Lox}$ mice, in which *Arl13b* exon 2 is flanked by LoxP sites (Su et al., 2012), with either *Nkx2.1-Cre* (Xu et al., 2008), *Ai3* (Stachniak et al., 2014) mice or *Parv-Cre* (Hippenmeyer et al., 2005), *Ai9* (Stachniak et al., 2014) mice. The Sstr3 expression was induced in *Arl13b* deleted interneurons by crossing *Arl13b*$^{lox/lox}$, *Nkx2.1-Cre* mice with Cre inducible *Sstr3GFP* (O'Connor et al., 2013), *Ai9* mice (Stachniak et al., 2014). Littermate *Arl13b*$^{lox/+}$, *Cre*$^{+}$ mice served as controls. Both males and females were used in all of the experiments.

METHOD DETAILS

Cilia targeted DREADD, calcium indicators, Sstr3 mutant, and human ARL13B variants

The cilia targeted DREADD (Cilia-hM3D$_q$) was generated by ligating a cilia-targeting-sequence [CLVCCWFKKSKTRKIKP; (Follit et al., 2010)] to the C-terminal of hM3D-mCitrine in a modified pcDNA3.1 vector containing CAG promoter (gift from Dr. Bryan Roth, University of North Carolina). The cilia targeted calcium indicator and GFP [Cilia-GECO1.0 and Cilia-GFP (Su et al., 2013)] are gifts from Dr. Takanari Inoue (John Hopkins University). Myc tagged D124E Sstr3 mutant in pcDNA3.1 vector is a gift from Dr. Kirk Mykytyn (Ohio State University, Green et al., 2016). The Cre-inducible adeno-associated virus (AAV) vectors expressing ARL13B variants and mCherry were generated using a pAAV-DIO-EF1a shuttle vector as described in Cardin et al., 2010 (Cardin et al., 2010). Each ARL13B variant (ARL13B, R79A, W82X, Y86C, R200C, mV358A; Higginbotham et al., 2012b) and mCherry were inserted into AAV-DIO-EF1a vector under the control of loxP sites.

In utero electroporation and ciliary calcium imaging

Lateral ventricles of embryonic day 14.5 control and littermate *Nkx2.1-Arl13b* mouse embryos were electroporated as described previously (Guo et al., 2015; Higginbotham et al., 2012b). Briefly, 1–2 μl of Cilia-GECO1.0 plasmid DNA (2 μg/μl) were injected into the lateral ventricles of E16.5 brains and electroporated using 5 pulses at 30 V for 50ms at 950ms intervals through the uterine wall using a BTX ElectroSquarePorator (ECM 830). Embryos were then allowed to develop *in vivo*. Cortices were removed from the

electroporated pups at P0, coronally sectioned (250 μm) in a vibratome (Leica VT 1000S), mounted on nucleopore membrane filters, placed in glass-bottom FluoroDish chambers (World Precision Instruments, Inc.) and maintained in neuralbasal/B27/L-Glutamine/ GlutaMax^{TM-I} medium at 37°C/5% CO_2. Striatal interneuronal (Ai9$^+$) primary cilia (GECO1.0$^+$) were repeatedly imaged at 20 seconds intervals using a Zeiss780 live cell confocal laser scanning system. Changes in ciliary Ca^{2+} indicator intensity were quantified and analyzed using Zeiss LSM Image Browser or ImageJ software (Higginbotham et al., 2012a; Yokota et al., 2007). Plasmids used for *in utero* electroporation were prepared using the EndoFree Plasmid kit (Qiagen).

AAV injections

AAV viruses (AAV2-FLEX-tdTomato) were injected unilaterally into the striatum of control and *Nkx2.1-Arl13b* mice at P1. Briefly, animals were cold anesthetized and 100nl of the viruses (10^{12} GC/ml) were injected over a 1-min period using a Hamilton microliter syringe (32 gauge needle) attached to an injection apparatus (World Precision Instruments). The needle was held in place for 1 min after each injection before slow retraction. Neuronal morphology and synaptic connections were analyzed at P30.

Cell lines and transfection

Mouse embryonic fibroblast (MEF) cells were derived from wild type and *Arl13b$^{hnn/hnn}$* E11.5 embryos as previously described (Higginbotham et al., 2012). Mouse kidney inner medullary collecting duct (IMCD3, CRL-2123) epithelial cells and MEF cells were grown in DMEM/F12 media supplemented with 10% fetal bovine serum (FBS) and 1% penicillin/ streptomycin (P/S) at 37°C/5% CO_2. Cells were allowed to reach 80% confluency and ciliogenesis was induced by serum starvation for 24 hours. Cells were then transfected using Invitrogen Lipofectamine 2000 reagent according to manufacture's instructions. Sex of the cell lines are unknown.

Primary interneuron culture and transfection

Medial ganglionic eminence from E15.5 *Arl13b$^{lox/+}$; Nkx2.1Cre; Ai9* or *Arl13b$^{lox/lox}$; Nkx2.1Cre; Ai9* embryos were dissociated and plated (20,000 cells/cm^2) on laminin/poly-L-lysine coated glass covers slips in Neurobasal-A/5% B27/1% GlutaMax/1% P/S media. Transfection of interneurons was performed using Invitrogen Lipofectamine 2000 according to manufacture's instructions. Some of the cultures were supplemented with SAG (200 nM; Calbiochem) or recombinant mouse Shh N-terminus (10μg/ml; R&D Systems). Sex of the embryos were not determined.

Ca^{2+} imaging *in vitro*

Interneurons or MEFs were transfected with Cilia-GECO1.0, and or Cilia-DREADDs and imaged at an acquisition rate of 0.5 Hz using a Zeiss 780 live cell confocal microscope. Cells were maintained in DMEM (Gibco) containing 0.9 mM Ca^{2+}. The effects of ATP or CNO were assessed by recording for 3 min before and after addition. GECO1.0 fluorescence values were normalized against background and to the average baseline values measured

prior to ATP or CNO addition. Image analysis was performed using Zeiss LSM Image Browser or ImageJ software.

Immunohistochemistry

Mouse brains were fixed with 4% paraformaldehyde, embedded in 3% agarose and sectioned (50 μm thick) with a Vibratome (VT1000S; Leica Microsystems). Neuronal cultures were fixed in 4% paraformaldehyde for 30 minutes. Sections and cells were blocked with PBS/10% goat serum/0.2% Triton X-100 for 1 h, and incubated in primary antibodies overnight at 4 °C or 3 hours at room temperature. The primary antibodies used were anti-GFP (chicken, 1:1000; Abcam, ab13970), anti-RFP (rabbit, 1:500; Rockland, cat. nr. 600-401-379), anti-Caspase 3 (rabbit, 1:1000; Millipore, ab3623), anti-PH3 (rabbit polyclonal, 1:1000; Millipore, cat. nr. 07-424), anti-Arl13b (mouse, 1:500; NeuroMabs, cat. nr. 75-287), anti-Sstr3 (goat, 1:100; Santa Cruz, sc-11617), anti-5ht6 (rabbit, 1:1000, Abcam, ab103016), anti-MCHR1 (goat, 1:100; Santa Cruz, sc-5534), anti-ACIII (rabbit polyclonal, 1:100; Santa Cruz, sc-56855), anti-PV (rabbit, 1:1000, Millipore, AB15736), anti-PV (mouse, 1:1000; Millipore, MAB1572), anti-SST (rat, 1:500, Millipore, MAB354), anti-Calretinin (rabbit, 1:500; Abcam, ab702), anti-VGAT (rabbit, 1:1000; Synaptic System, cat. nr. 131003), anti-NeuN (mouse, 1:1000, Millipore, MAB377). After three washes in 1×PBS, sections and cells were incubated with secondary antibodies (1:1,000) at room temperature for 2 h, washed and mounted with Citifluor anti-fading solution (Agar). AlexaFluor 488, 647 or Cy3-conjugated (Invitrogen and Jackson ImmunoResearch) secondary antibodies were used. Nuclei were counterstained with DAPI (Sigma).

Patch Clamp Electrophysiology

Mice were anesthetized with pentobarbital and transcardial perfusions were performed using an ice-cold sucrose cutting solution containing the following (in mM): 225 sucrose, 119 NaCl, 1.0 NaH_2P0_4, 4.9 $MgCl_2$, 0.1 $CaCl_2$, 26.2 $NaHCO_3$, 1.25 glucose, 305 mOsm. Brains were then removed and submerged in the cutting solution, while coronal sections 300μm thick were taken using a vibrating blade (Leica, VT 1200). Slices were then placed in warm aCSF (32°C) containing the following (in mM): 119 NaCl, 2.5 KCl, 1.0 NaH_2P0_4, 1.3 MgCl, 2.5 $CaCl_2$, 26.2 $NaHCO_3$, 15 glucose, 305 mOsm. After one hour of recovery, slices were perfused with warm aCSF (32°C) containing 1 μM tetrodotoxin (Sigma-Aldrich). Neurons were visualized using differential interference contrast through an upright 40x water-immersion objective mounted on an upright microscope (Olympus BX51WI). Fluorescent imaging using a mercury lamp (Olympus U-RFL-T) was used to identify striatal $tdTomato^+$ interneurons. TdTomato negative medium spiny neurons were identified by their characteristic late spiking firing pattern. Voltage-clamp recordings were obtained using glass electrodes (3–5 MΩ) back-filled with cesium methylsulfonate internal solution containing of the following (in mM): 117 Cs methanesulfonic acid, 20 HEPES, 2.8 NaCl, 5 TEA, 2 ATP, 0.2 GTP, pH 7.35, mOsm 280. mEPSCs were obtained by holding neurons at -70mV for 5 minutes, whereas mIPSCs were obtained by holding neurons at +40mV for 5 minutes. Data acquisition occurred at 1 kHz sampling rate through a MultiClamp 700B amplifier connected to a Digidata 1440A digitizer (Molecular Devices). Additional details on patch-clamp recordings are available in Otis et al., 2014. Data were analyzed using a template

analysis (Clampfit 10.3). Excitatory/inhibitory ratio was calculated as follows: (mEPSC frequency x mEPSC amplitude)/(mIPSC frequency x mIPSC amplitude).

QUANTIFICATION AND STATISTICAL ANALYSIS

GraphPad or Excel was used for data analysis. Two-tailed Student's *t* test and ANOVA test were performed using GraphPad. Data were collected and processed blindly. All experiments were independently repeated for at least 3 or more times. All data are expressed as means ± standard error of the mean (SEM). Statistical details are included in figure legends.

Supplementary Material

Refer to Web version on PubMed Central for supplementary material.

Acknowledgments

This research was supported by NIH grants NS 090029 and MH060929 to E.S.A and by the confocal imaging core of an NINDS institutional center core grant (5P30NS045892). We thank Dr. B. Roth (UNC) and Dr. B. Yoder (The Hepatorenal Fibrocystic Disease Core Center, UAB [DK074038]) for assistance with reagents and helpful comments. The authors declare no competing financial interests.

References

Adamantidis A, Thomas E, Foidart A, Tyhon A, Coumans B, Minet A, Tirelli E, Seutin V, Grisar T, Lakaye B. Disrupting the melanin-concentrating hormone receptor 1 in mice leads to cognitive deficits and alterations of NMDA receptor function. The European journal of neuroscience. 2005; 21:2837–2844. [PubMed: 15926931]

Alvarez Retuerto AI, Cantor RM, Gleeson JG, Ustaszewska A, Schackwitz WS, Pennacchio LA, Geschwind DH. Association of common variants in the Joubert syndrome gene (AHI1) with autism. Human Molecular Genetics. 2008; 17:3887–3896. [PubMed: 18782849]

Amann-Zalcenstein D, Avidan N, Kanyas K, Ebstein RP, Kohn Y, Hamdan A, Ben-Asher E, Karni O, Mujaheed M, Segman RH, et al. AHI1, a pivotal neurodevelopmental gene, and C6orf217 are associated with susceptibility to schizophrenia. European journal of human genetics: EJHG. 2006; 14:1111–1119. [PubMed: 16773125]

Armbruster BA, Li X, Pausch MH, Herlitze S, Roth BL. Evolving the lock to fit the key to create a family of G protein-coupled receptors potently activated by an inert ligand. Proc Natl Acad Sci U S A. 2007; 104:5163–5168. [PubMed: 17360345]

Baraban SC, Southwell DG, Estrada RC, Jones DL, Sebe JY, Alfaro-Cervello C, García-Verdugo JM, Rubenstein JLR, Alvarez-Buylla A. Reduction of seizures by transplantation of cortical GABAergic interneuron precursors into Kv1.1 mutant mice. Proc Natl Acad Sci U S A. 2009; 106:15472–15477. [PubMed: 19706400]

Badgandi HB, Hwang SH, Shimada IS, Loriot E, Mukhopadhyay S. Tubby family proteins are adapters for ciliary trafficking of integral membrane proteins. Journal of Cell Biology. 2017; 216:743–760. [PubMed: 28154160]

Baudoin JP, Viou L, Launay PS, Luccardini C, Espeso Gil S, Kiyasova V, Irinopoulou T, Alvarez C, Rio JP, Boudier T, Lechaire JP, Kessaris N, Spassky N, Métin C. Tangentially migrating neurons assemble a primary cilium that promotes their reorientation to the cortical plate. Neuron. 2012; 76:1108–22. [PubMed: 23259947]

Belgacem YH, Borodinsky LN. Sonic hedgehog signaling is decoded by calcium spike activity in the developing spinal cord. Proceedings of the National Academy of Sciences. 2011; 108:4482–4487.

Berbari NF, Johnson AD, Lewis JS, Askwith CC, Mykytyn K. Identification of ciliary localization sequences within the third intracellular loop of G protein-coupled receptors. Molecular Biology of the Cell. 2008; 19:1540–1547. [PubMed: 18256283]

Betley JN, Wright CVE, Kawaguchi Y, Erdélyi F, Szabó G, Jessell TM, Kaltschmidt JA. Stringent specificity in the construction of a GABAergic presynaptic inhibitory circuit. Cell. 2009; 139:161–174. [PubMed: 19804761]

Bourgeron T. A synaptic trek to autism. Current opinion in neurobiology. 2009; 19:231–234. [PubMed: 19545994]

Brailov I, Bancila M, Brisorgueil MJ, Miquel MC, Hamon M, Vergé D. Localization of 5-HT(6) receptors at the plasma membrane of neuronal cilia in the rat brain. Brain research. 2000; 872:271–275. [PubMed: 10924708]

Brear AG, Yoon J, Wojtyniak M, Sengupta P. Diverse cell type-specific mechanisms localize G protein-coupled receptors to Caenorhabditis elegans sensory cilia. Genetics. 2014; 197:667–684. [PubMed: 24646679]

Cantagrel V, Silhavy JL, Bielas SL, Swistun D, Marsh SE, Bertrand JY, Audollent S, Atti-Bitach T, Holden KR, Dobyns WB, et al. Mutations in the Cilia Gene ARL13B Lead to the Classical Form of Joubert Syndrome. The American Journal of Human Genetics. 2008; 83:170–179. [PubMed: 18674751]

Caspary T, Larkins CE, Anderson KV. The graded response to Sonic Hedgehog depends on cilia architecture. Developmental Cell. 2007; 12:767–778. [PubMed: 17488627]

Cevik S, Hori Y, Kaplan OI, Kida K, Toivenon T, Foley-Fisher C, Cottell D, Katada T, Kontani K, Blacque OE. Joubert syndrome Arl13b functions at ciliary membranes and stabilizes protein transport in Caenorhabditis elegans. J Cell Biol. 2010; 188:953–969. [PubMed: 20231383]

Chattopadhyaya B, Di Cristo G, Higashiyama H, Knott GW, Kuhlman SJ, Welker E, Huang ZJ. Experience and activity-dependent maturation of perisomatic GABAergic innervation in primary visual cortex during a postnatal critical period. J Neurosci. 2004; 24:9598–9611. [PubMed: 15509747]

Chattopadhyaya B, Di Cristo G, Wu CZ, Knott G, Kuhlman S, Fu Y, Palmiter RD, Huang ZJ. GAD67-mediated GABA synthesis and signaling regulate inhibitory synaptic innervation in the visual cortex. Neuron. 2007; 54:889–903. [PubMed: 17582330]

Chattopadhyaya B. Molecular mechanisms underlying activity-dependent GABAergic synapse development and plasticity and its implications for neurodevelopmental disorders. Neural plasticity. 2011; 2011:734231. [PubMed: 21826279]

Clark L, Chamberlain SR, Sahakian BJ. Neurocognitive mechanisms in depression: implications for treatment. Annual review of neuroscience. 2009; 32:57–74.

Close J, Xu H, De Marco García N, Batista-Brito R, Rossignol E, Rudy B, Fishell G. Satb1 is an activity-modulated transcription factor required for the terminal differentiation and connectivity of medial ganglionic eminence-derived cortical interneurons. J Neurosci. 2012; 32:17690–17705. [PubMed: 23223290]

Smoller JW, Craddock N, Kendler K, Lee PH, Neale BM, Nurnberger JI, Ripke S, Santangelo S, Sullivan PF. Consortium C.-D.G.o.t.P.G. Identification of risk loci with shared effects on five major psychiatric disorders: a genome-wide analysis. Lancet. 2013; 381:1371–1379. [PubMed: 23453885]

Consortium, N.a.P.A.S.o.t.P.G, (IIBDGC), I.I.B.D.G.C., and IIBDGC, I.I.B.D.G.C. Psychiatric genome-wide association study analyses implicate neuronal, immune and histone pathways. Nature neuroscience. 2015; 18:199–209. [PubMed: 25599223]

De Marco García NV, Karayannis T, Fishell G. Neuronal activity is required for the development of specific cortical interneuron subtypes. Nature. 2011; 472:351–355. [PubMed: 21460837]

De Marco García NV, Priya R, Tuncdemir SN, Fishell G, Karayannis T. Sensory inputs control the integration of neurogliaform interneurons into cortical circuits. Nature neuroscience. 2015; 18:393–401. [PubMed: 25664912]

DeCaen PG, Delling M, Vien TN, Clapham DE. Direct recording and molecular identification of the calcium channel of primary cilia. Nature. 2013; 504:315–318. [PubMed: 24336289]

Dehorter N, Ciceri G, Bartolini G, Lim L, del Pino I, Marín O. Tuning of fast-spiking interneuron properties by an activity-dependent transcriptional switch. Science. 2015; 349:1216–20. [PubMed: 26359400]

Delling M, DeCaen PG, Doerner JF, Febvay S, Clapham DE. Primary cilia are specialized calcium signalling organelles. Nature. 2013; 504:311–314. [PubMed: 24336288]

Denaxa M, Kalaitzidou M, Garefalaki A, Achimastou A, Lasrado R, Maes T, Pachnis V. Maturation-promoting activity of SATB1 in MGE-derived cortical interneurons. Cell Reports. 2012; 2:1351–1362. [PubMed: 23142661]

Donato F, Rompani SB, Caroni P. Parvalbumin-expressing basket-cell network plasticity induced by experience regulates adult learning. Nature. 2013; 504:272–276. [PubMed: 24336286]

Dong S, Allen JA, Farrell M, Roth BL. A chemical-genetic approach for precise spatio-temporal control of cellular signaling. Molecular Biosystems. 2010; 6:1376–1380. [PubMed: 20532295]

Einstein EB, Patterson CA, Hon BJ, Regan KA, Reddi J, Melnikoff DE, Mateer MJ, Schulz S, Johnson BN, Tallent MK. Somatostatin signaling in neuronal cilia is critical for object recognition memory. J Neurosci. 2010; 30:4306–4314. [PubMed: 20335466]

Evans AE, Kelly CM, Precious SV, Rosser AE. Molecular regulation of striatal development: a review. Anatomy Research International. 2012; 2012:106529. [PubMed: 22567304]

Fazzari P, Paternain AV, Valiente M, Pla R, Luján R, Lloyd K, Lerma J, Marín O, Rico B. Control of cortical GABA circuitry development by Nrg1 and ErbB4 signalling. Nature. 2010; 464:1376–80. [PubMed: 20393464]

Flames N, Long JE, Garratt AN, Fischer TM, Gassmann M, Birchmeier C, Lai C, Rubenstein JL, Marín O. Short- and long-range attraction of cortical GABAergic interneurons by neuregulin-1. Neuron. 2004; 44:251–61. [PubMed: 15473965]

Follit JA, Li L, Vucica Y, Pazour GJ. The cytoplasmic tail of fibrocystin contains a ciliary targeting sequence. The Journal of cell biology. 2010; 188:21–28. [PubMed: 20048263]

Gittis AH, Kreitzer AC. Striatal microcircuitry and movement disorders. Trends in Neurosciences. 2012; 35:557–564. [PubMed: 22858522]

Green JA, Gu C, Mykytyn K. Heteromerization of ciliary G protein-coupled receptors in the mouse brain. PloS one. 2012; 7:e46304. [PubMed: 23029470]

Green JA, Mykytyn K. Neuronal primary cilia: an underappreciated signaling and sensory organelle in the brain. Neuropsychopharmacology: official publication of the American College of Neuropsychopharmacology. 2014; 39:244–245. [PubMed: 24317320]

Green JA, Schmid CL, Bley E, Monsma PC, Browon A, Bohn LM, Mykytyn K. Recruitment of b-arrestin into neuronal cilia modulates somatostatin receptor subtype 3 ciliary localization. Mol Cell Biol. 2016; 36:223–235. [PubMed: 26503786]

Guemez-Gamboa A, Coufal NG, Gleeson JG. Primary Cilia in the Developing and Mature Brain. Neuron. 2014; 82:511–521. [PubMed: 24811376]

Guo J, Anton ES. Decision making during interneuron migration in the developing cerebral cortex. Trends in cell biology. 2014

Guo J, Higginbotham H, Li J, Nichols J, Hirt J, Ghukasyan V, Anton ES. Developmental disruptions underlying brain abnormalities in ciliopathies. Nature Communications. 2015; 6:7857.

Händel M, Schulz S, Stanarius A, Schreff M, Erdtmann-Vourliotis M, Schmidt H, Wolf G, Höllt V. Selective targeting of somatostatin receptor 3 to neuronal cilia. Neuroscience. 1999; 89:909–926. [PubMed: 10199624]

Harwell CC, Parker PRL, Gee SM, Okada A, McConnell SK, Kreitzer AC, Kriegstein AR. Sonic hedgehog expression in corticofugal projection neurons directs cortical microcircuit formation. Neuron. 2012; 73:1116–1126. [PubMed: 22445340]

Higginbotham H, Eom TY, Mariani LE, Bachleda A, Hirt J, Gukassyan V, Cusack CL, Lai C, Caspary T, Anton ES. Arl13b in Primary Cilia Regulates the Migration and Placement of Interneurons in the Developing Cerebral Cortex. Developmental Cell. 2012; 23:925–938. [PubMed: 23153492]

Higginbotham H, Guo J, Yokota Y, Umberger NL, Su CY, Li J, Verma N, Hirt J, Ghukasyan V, Caspary T, et al. Arl13b-regulated cilia activities are essential for polarized radial glial scaffold formation. Nature neuroscience. 2013; 16:1000–1007. [PubMed: 23817546]

Hildebrandt F, Benzing T, Katsanis N. Ciliopathies. The New England journal of medicine. 2011; 364:1533–1543. [PubMed: 21506742]

Hippenmeyer S, Vrieseling E, Sigrist M, Portmann T, Laengle C, Ladle DR, Arber S. A developmental switch in the response of DRG neurons to ETS transcription factor signaling. PLOS Biology. 2005; 3:e159. [PubMed: 15836427]

Humbert MC, Weihbrecht K, Searby CC, Li Y, Pope RM, Sheffield VC, Seo S. ARL13B, PDE6D, and CEP164 form a functional network for INPP5E ciliary targeting. Proc Natl Acad Sci U S A. 2012; 109:19691–19696. [PubMed: 23150559]

Hwang SH, Mukhopadhyay S. G-protein-coupled receptors and localized signaling in the primary cilium during ventral neural tube patterning. Birth defects research Part A, Clinical and molecular teratology. 2015; 103:12–19. [PubMed: 24917297]

Karnani MM, Jackson J, Ayzenshtat I, Tucciarone J, Manoocheri K, Snider WG, Yuste R. Cooperative Subnetworks of Molecularly Similar Interneurons in Mouse Neocortex. Neuron. 2016; 90:86–100. [PubMed: 27021171]

Kepecs A, Fishell G. Interneuron cell types are fit to function. Nature. 2014; 505:318. [PubMed: 24429630]

Kinney JW, Davis CN, Tabarean I, Conti B, Bartfai T, Behrens MM. A specific role for NR2A-containing NMDA receptors in the maintenance of parvalbumin and GAD67 immunoreactivity in cultured interneurons. J Neurosci. 2006; 26:1604–1615. [PubMed: 16452684]

Korotkova T, Fuchs EC, Ponomarenko A, von Engelhardt J, Monyer H. NMDA receptor ablation on parvalbumin-positive interneurons impairs hippocampal synchrony, spatial representations, and working memory. Neuron. 2010; 68:557–569. [PubMed: 21040854]

Lee JE, Gleeson JG. Cilia in the nervous system: linking cilia function and neurodevelopmental disorders. Current Opinion in Neurology. 2011; 24:98–105. [PubMed: 21386674]

Lehtinen MK, Zappaterra MW, Chen X, Yang YJ, Hill AD, Lun M, Maynard T, Gonzalez D, Kim S, Ye P, et al. The cerebrospinal fluid provides a proliferative niche for neural progenitor cells. Neuron. 2011; 69:893–905. [PubMed: 21382550]

Loktev AV, Jackson PK. Neuropeptide Y Family Receptors Traffic via the Bardet-Biedl Syndrome Pathway to Signal in Neuronal Primary Cilia. Cell Reports. 2013; 5:1316–1329. [PubMed: 24316073]

Louvi A, Grove EA. Cilia in the CNS: the quiet organelle claims center stage. Neuron. 2011; 69:1046–1060. [PubMed: 21435552]

Mardinly AR, Spiegel I, Patrizi A, Centofante E, Bazinet JE, Tzeng CP, Mandel-Brehm C, Harmin DA, Adesnik H, Fagiolini M, et al. Sensory experience regulates cortical inhibition by inducing IGF1 in VIP neurons. Nature. 2016; 531:371–375. [PubMed: 26958833]

Marín O. Interneuron dysfunction in psychiatric disorders. Nature Reviews Neuroscience. 2012; 13:107–120. [PubMed: 22251963]

Marín O. Cellular and molecular mechanisms controlling the migration of neocortical interneurons. The European Journal of Neuroscience. 2013; 38:2019–2029. [PubMed: 23651101]

Marley A, Choy RWY, von Zastrow M. GPR88 reveals a discrete function of primary cilia as selective insulators of GPCR cross-talk. PloS one. 2013; 8:e70857. [PubMed: 23936473]

Marley A, Von Zastrow M. A simple cell-based assay reveals that diverse neuropsychiatric risk genes converge on primary cilia. PLoS ONE. 2012; 7:e46647. [PubMed: 23056384]

Maroof AM, Keros S, Tyson JA, Ying SW, Ganat YM, Merkle FT, Liu B, Goulburn A, Stanley EG, Elefanty AG, et al. Directed differentiation and functional maturation of cortical interneurons from human embryonic stem cells. Cell stem cell. 2013; 12:559–572. [PubMed: 23642365]

Miertzschke M, Koerner C, Spoerner M, Wittinghofer A. Structural insights into the small G-protein Arl13B and implications for Joubert syndrome. The Biochemical journal. 2014; 457:301–311. [PubMed: 24168557]

Miyoshi K, Kasahara K, Miyazaki I, Asanuma M. Lithium treatment elongates primary cilia in the mouse brain and in cultured cells. Biochemical and biophysical research communications. 2009; 388:757–762. [PubMed: 19703416]

Nager AR, Goldstein JS, Herranz-Pe'rez V, Portran D, Ye F, Garcia-Verdugo JM, Nachury MV. An actin network dispatches ciliary GPCRs into extracellular vesicles to modulate signaling. Cell. 2017; 168:252–263. [PubMed: 28017328]

O'Connor AK, Malarkey EB, Berbari NF, Croyle MJ, Haycraft CJ, Bell PD, Hohenstein P, Kesterson RA, Yoder BK. An inducible CiliaGFP mouse model for in vivo visualization and analysis of cilia in live tissue. Cilia. 2013; 2:8. [PubMed: 23819925]

Omori Y, Chaya T, Yoshida S, Irie S, Tsujii T, Furukawa T. Identification of G Protein-Coupled Receptors (GPCRs) in primary cilia and their possible involvement in body weight control. PloS one. 2015; 10:e0128422. [PubMed: 26053317]

Otis JM, Fitzgerald MK, Mueller D. Infralimbic BDNF/TrkB enhancement of GluN2B currents facilitates extinction of a cocaine-conditioned place preference. J Neurosci. 2014; 34:6057–6064. [PubMed: 24760865]

Parikshak NN, Luo R, Zhang A, Won H, Lowe JK, Chandran V, Horvath S, Geschwind DH. Integrative functional genomic analyses implicate specific molecular pathways and circuits in autism. Cell. 2013; 155:1008–1021. [PubMed: 24267887]

Pieraut S, Gounko N, Sando R, Dang W, Rebboah E, Panda S, Madisen L, Zeng H, Maximov A. Experience-dependent remodeling of basket cell networks in the dentate gyrus. Neuron. 2014; 84:107–122. [PubMed: 25277456]

Qiu C, Zeyda T, Johnson B, Hochgeschwender U, deLecea L, Tallent MK. Somatostatin receptor subtype4 couples to the M-current to regulate seizures. J Neurosci. 2008; 28:3567–3576. [PubMed: 18385315]

Shepherd GMG. Corticostriatal connectivity and its role in disease. Nature reviews Neuroscience. 2013; 14:278–291. [PubMed: 23511908]

Soetedjo L, Glover DvA, Jin H. Targeting of vasoactive intestinal peptide receptor 2, VPAC2, a secretin family G-protein coupled receptor, to primary cilia. Biology open. 2013; 2:686–694. [PubMed: 23862016]

Southwell DG, Froemke RC, Alvarez-Buylla A, Stryker MP, Gandhi SP. Cortical plasticity induced by inhibitory neuron transplantation. Science (New York, NY). 2010; 327:1145–1148.

Stachniak TJ, Ghosh A, Sternson SM. Chemogenetic synaptic silencing of neural circuits localizes a hypothalamus→midbrain pathway for feeding behavior. Neuron. 2014; 82:797–808. [PubMed: 24768300]

Stepanek L, Pigino G. Microtubule doublets are double-track railways for intraflagellar transport trains. Science. 2016; 352:721–724. [PubMed: 27151870]

Su CY, Bay SN, Mariani LE, Hillman MJ, Caspary T. Temporal deletion of Arl13b reveals that a mispatterned neural tube corrects cell fate over time. Development (Cambridge, England). 2012; 139:4062–4071.

Su S, Phua SC, Derose R, Chiba S, Narita K, Kalugin PN, Katada T, Kontani K, Takeda S, Inoue T. Genetically encoded calcium indicator illuminates calcium dynamics in primary cilia. Nature methods. 2013; 10:1105. [PubMed: 24056873]

Svenningsson P, Tzavara ET, Qi H, Carruthers R, Witkin JM, Nomikos GG, Greengard P. Biochemical and behavioral evidence for antidepressant-like effects of 5-HT6 receptor stimulation. J Neurosci. 2007; 27:4201–4209. [PubMed: 17428998]

Thomas S, Cantagrel V, Mariani L, Serre V, Lee JE, Elkhartoufi N, de Lonlay P, Desguerre I, Munnich A, Boddaert N, et al. Identification of a novel ARL13B variant in a Joubert syndrome-affected patient with retinal impairment and obesity. European journal of human genetics: EJHG. 2015; 23:621–627. [PubMed: 25138100]

Touzot A, Ruiz-Reig N, Vitalis T, Studer M. Molecular control of two novel migratory paths for CGE-derived interneurons in the developing mouse brain. Development. 2016; 143:1753–1765. [PubMed: 27034423]

Viollet C, Lepousez G, Loudes C, Videau C, Simon A, Epelbaum J. Somatostatinergic systems in brain: networks and functions. Molecular and cellular endocrinology. 2008; 286:75–87. [PubMed: 17997029]

Voineagu I, Wang X, Johnston P, Lowe JK, Tian Y, Horvath S, Mill J, Cantor RM, Blencowe BJ, Geschwind DH. Transcriptomic analysis of autistic brain reveals convergent molecular pathology. Nature. 2011; 474:380–384. [PubMed: 21614001]

Xu Q, Tam M, Anderson SA. Fate mapping Nkx2.1-lineage cells in the mouse telencephalon. The Journal of Comparative Neurology. 2008; 506:16–29. [PubMed: 17990269]

Xu Q, Wonders CP, Anderson SA. Sonic hedgehog maintains the identity of cortical interneuron progenitors in the ventral telencephalon Nkx2.1-lineage cells in the mouse telencephalon. Development. 2005; 132:4987–4998. [PubMed: 16221724]

Highlights

- Primary cilia signaling regulates interneuronal morphology and synaptic connectivity
- Ciliary GPCR signaling is critical for emergence of interneuronal connectivity.
- Cilia signaling is a non-synaptic mechanism to sculpt interneuronal circuits.
- Disrupted cilia signaling may underlie circuit malformations in ciliopathies

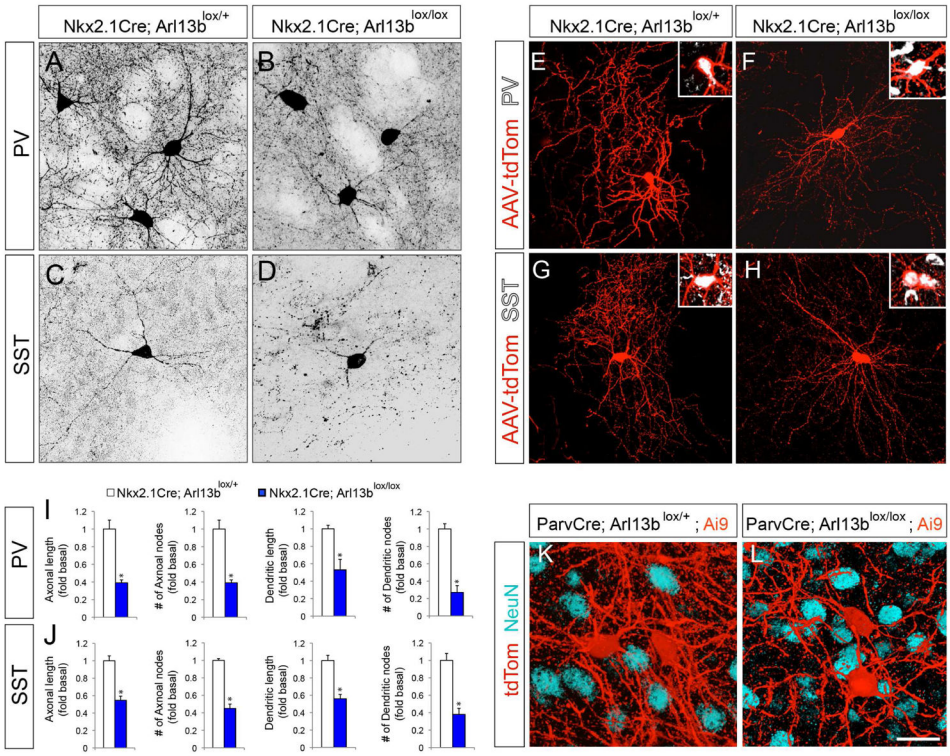

Figure 1. Deletion of Arl13b in interneurons results in morphological defects

(A–B) Striatal PV$^+$ interneurons were labeled with anti-PV antibodies in *Nkx2.1Cre; Arl13b$^{lox/+}$* (A) and *Nkx2.1Cre; Arl13b$^{lox/lox}$* (B) brains. (C, D) Striatal SST$^+$ INs were labeled with anti-SST antibody in *Nkx2.1Cre; Arl13b$^{lox/+}$* (C) and *Nkx2.1 Cre; Arl13b$^{lox/lox}$* (D) brains. (E–H) Representative images of PV$^+$ (E, F) or SST$^+$ INs (G, H) interneurons from AAV2-FLEX-tdTomato injected *Nkx2.1Cre; Arl13b$^{lox/+}$* (E, G) and *Nkx2.1Cre; Arl13b$^{lox/lox}$* (F, H) brains. Insets (E–H) show co-labeling of tdTom$^+$ neurons with PV (E, F) and SST (G, H) antibodies. (I–J) Quantification of morphological defects of PV$^+$ (I) and SST$^+$ (J) INs in *Nkx2.1Cre; Arl13b$^{lox/lox}$* brains [P30]. Data shown are mean ± SEM. $^*P<0.05$ (Student's *t*-test;). (K–L) Representative images of tdTom$^+$ INs from *ParvCre; Arl13b$^{lox/+}$; Ai9* (K) and *ParvCre; Arl13b$^{lox/lox}$; Ai9* (L) brains [P60]. Neurons were co-labeled with anti-NeuN antibodies. Data shown are mean ± SEM. $^*P<0.05$ (Student's *t*-test, $p_{[PV^+ \text{ axonal length}]} = 5.32281E\text{-}06$, $p_{[PV^+ \text{ axonal node}]} = 0.0005$, $p_{[PV^+ \text{ dendritic length}]} = 0.0001$, $p_{[PV^+ \text{ dendritic node}]} = 0.0003$, $p_{[SST^+ \text{ axonal length}]} = 7.92531E\text{-}06$, $p_{[SST^+ \text{ axonal node}]} = 0.0002$, $p_{[SST^+ \text{ dendritic length}]} = 0.002$, $p_{[SST^+ \text{ dendritic node}]} = 0.0003$). 42 cells from 4 different brains were analyzed per group. Scale bar, 25μm (A–D); 50μm (E–H); 20μm (K, L). See also Figure S1, Figure S2, and Figure S3.

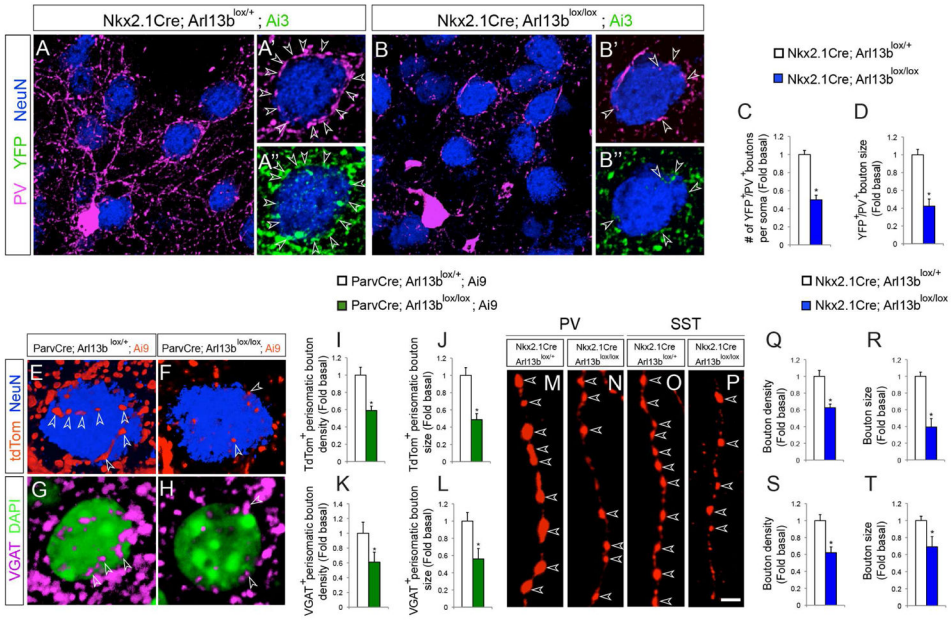

Figure 2. Changes in synaptic connectivity of Arl13b deficient interneurons

(A, B) Striatal neurons were labeled with anti-PV, anti-GFP, and anti-NeuN antibodies in *Nkx2.1Cre; Arl13b$^{lox/+}$; Ai3* (A) and *Nkx2.1Cre; Arl13b$^{lox/lox}$; Ai3* (B) brains. (A′, B′) PV$^+$ or YFP$^+$ perisomatic synaptic boutons (arrowheads) in control (A′, A″) and in *Nkx2.1Cre; Arl13b$^{lox/lox}$* (B′, B″) brains. Striatal medium spiny neurons (blue) are NeuN positive. (C, D) Quantification of PV$^+$ perisomatic bouton density and size in control and *Nkx2.1Cre; Arl13b$^{lox/lox}$; Ai3* brains [P30]. Data shown are mean ± SEM. $^*P<0.05$ (Student's *t*-test, $p_{[C]} = 0.0001$, $p_{[D]} = 0.0001$). (E–F) Representative images of striatal medium spiny neurons co-labeled with anti-NeuN antibodies in *ParvCre; Arl13b$^{lox/+}$; Ai9* (E) and *ParvCre; Arl13b$^{lox/lox}$; Ai9* (F) brains [P60]. Arrowheads indicate tdTom$^+$ perisomatic boutons. (G, H) Representative images of striatal medium spiny neurons co-labeled with anti-VGAT antibodies and DAPI in *ParvCre; Arl13b$^{lox/+}$; Ai9* (G) and *ParvCre; Arl13b$^{lox/lox}$; Ai9* (H) brains. Arrowheads (G–H) indicate VGAT$^+$ perisomatic boutons. (I–L) Quantification of PV$^+$ perisomatic bouton density and size in control and *ParvCre; Arl13b$^{lox/lox}$; Ai9* brains. Data shown are mean ± SEM. $^*P<0.05$ (Student's *t*-test, $p_{[I]} = 0.0001$, $p_{[J]} = 0.0004$, $p_{[K]} = 0.0003$, $p_{[L]} = 0.0003$). (M–P) tdTomato labeled PV$^+$ (M, N) and SST$^+$ (O, P) INs from AAV2-FLEX-tdTomato injected *Nkx2.1Cre; Arl13b$^{lox/+}$* (M, O) and *Nkx2.1Cre; Arl13b$^{lox/lox}$* (N, P) brains show synaptic boutons (arrowheads) along single axons. (Q–T) Quantification of the synaptic bouton density and size of PV$^+$ (Q, R) and SST$^+$ (S, T) INs in *Nkx2.1Cre; Arl13b$^{lox/lox}$* brains. Data shown are mean ± SEM. $^*P<0.05$ (Student's *t*-test, $p_{[Q]} = 0.003$, $p_{[R]} = 0.0004$, $p_{[S]} = 0.0001$, $p_{[T]} = 0.001$). 42 cells from 4 different brains were analyzed per group. Scale bar, 8.5μm (A, B); 4.3μm (A′, A″, B′, B″); 2.5μm (E–H); 2μm (M–P). See also Figure S2 and Figure S3.

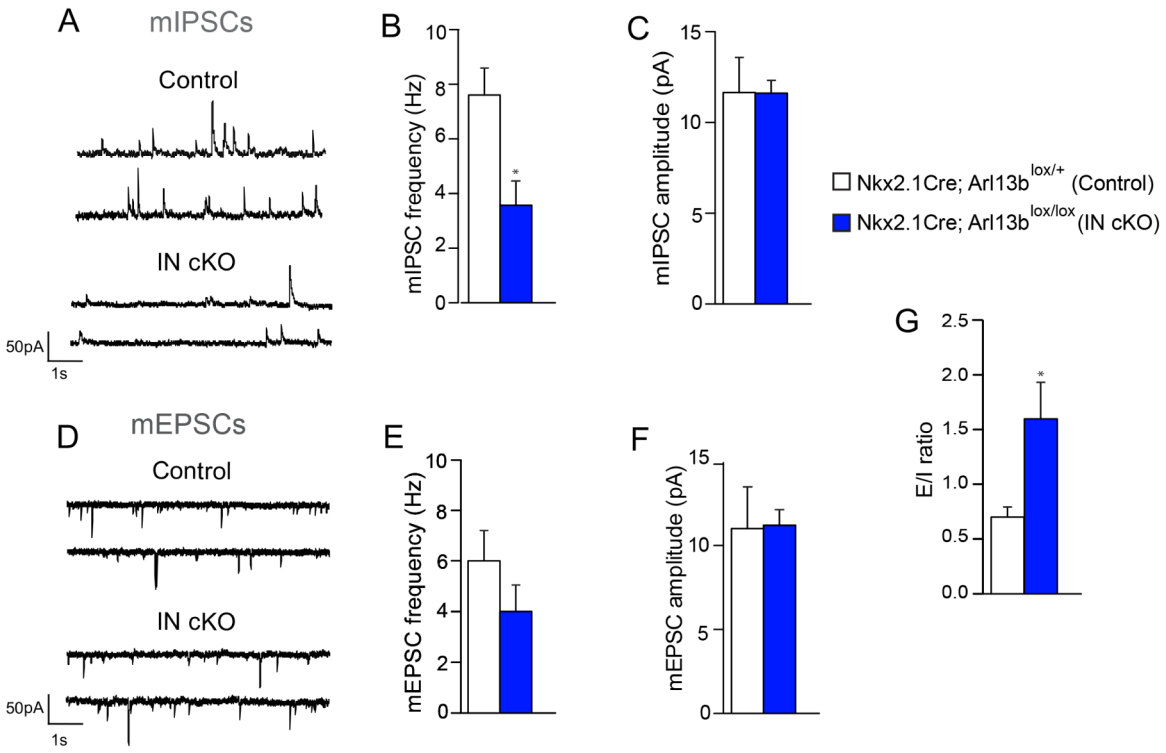

Figure 3. The functional impact of impaired primary cilia signaling in interneurons

(A) Representative patch-clamp electrophysiological recordings showing mIPSCs in striatal MSNs of *Nkx2.1Cre; Arl13b*$^{lox/+}$ (control) and *Nkx2.1Cre; Arl13b*$^{lox/lox}$ (IN cKO) mice. (B, C) Quantification of mIPSC frequency (B) and amplitude (C). $^{*}P<0.05$ (Student's *t*-test, mIPSC frequency: t(15) = 3.167, p = 0.0066; control, n=6; IN cKO, n =11). (D) Representative recordings showing mEPSCs in striatal MSNs of *Nkx2.1Cre; Arl13b*$^{lox/+}$ and *Nkx2.1Cre; Arl13b*$^{lox/lox}$ brains. (E, F) Quantification of mEPSC frequency (E) and amplitude (F). Data shown are mean ± SEM. (Student's *t*-test; mIPSC amplitude, mEPSC frequency, mEPSC amplitude: t-values <1). (G) Overall excitatory/inhibitory ratio in striatal MSNs of *Nkx2.1Cre; Arl13b*$^{lox/+}$ and *Nkx2.1Cre; Arl13b*$^{lox/lox}$ brains (Student's *t*-test: t(14)=2.277; p = 0.0390; control, n=6; IN cKO, n=10).

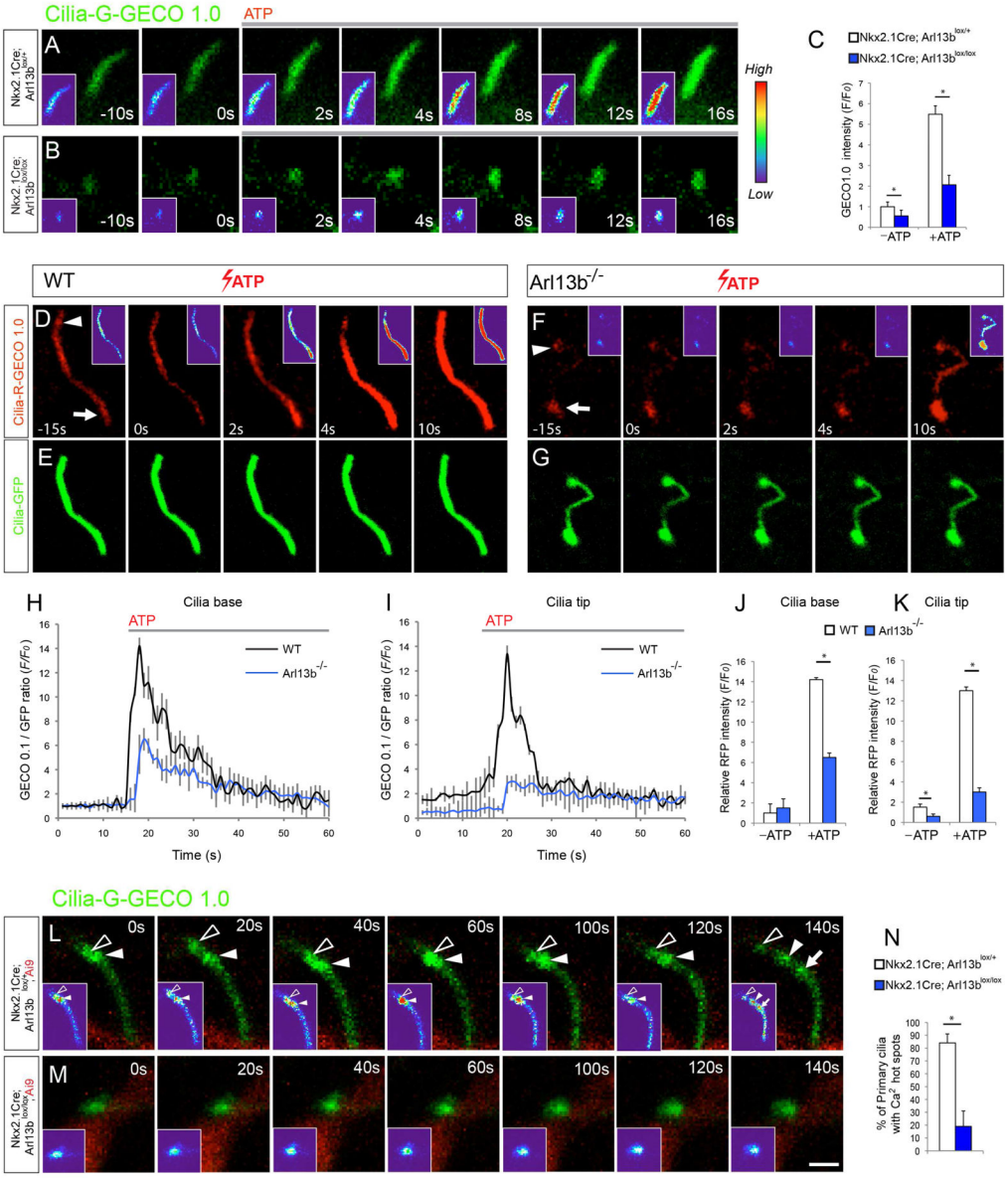

Figure 4. Defective calcium signaling in Arl13b deficient primary cilia

(A–B) Time-lapse imaging of interneurons from *Nkx2.1Cre; Arl13b*$^{lox/+}$ (A) and *Nkx2.1Cre; Arl13b*$^{lox/lox}$ (B) striatum expressing Cilia-G-GECO1.0. were treated with 10μM ATP. Insets (A–B) show changes in fluorescence intensity in pseudocolor (Red [High], Blue [Low]). (C) Quantification of changes in the fluorescence intensity of Cilia-G-GECO1.0 in control and mutant cilia. Data shown are mean ± SEM. $^{*}P<0.05$ (Student's *t*-test, $p_{[-ATP]} = 0.002$, $p_{[+ATP]} = 0.0004$). 15 neurons from 3 independent experiments were analyzed per group. (D–G) Time-lapse imaging of wild type (D, E) and Arl13b null (F, G) MEF cells expressing Cilia-R-GECO1.0 and Cilia-GFP treated with 10μM ATP. Arrowhead and arrow (D, F) indicate cilia tip and base, respectively. Insets (D, F) show fluorescence intensity in pseudocolor. (H, I) RFP fluorescence/GFP fluorescence ratio at cilia base (H) and tip (I) before and after administration of ATP in wild type (n=9) and Arl13b null cells

(n=11). Data shown are mean ± SEM. $^{*}P<0.05$ (Student's *t*-test, p = 0.002). (J, K) Changes in calcium indicator (GECO-RFP)/GFP fluorescence intensity at cilia base (Arrow [D, K]; J) and tip (Arrowhead [D, F]; K) before (−ATP, T=0) and after ATP (+ATP) in wild type (n=9) and Arl13b null cilia (n=11). Data shown are mean ± SEM. $^{*}P<0.05$ (Student's *t*-test, $p_{[J]}$ = 0.0006, $p_{[K]}$ = 0.0002). (L–M) Time-lapse imaging of spontaneous calcium dynamics in interneuronal primary cilia from *Nkx2.1Cre; Arl13b*$^{lox/+}$*; Ai9* (L) and *Nkx2.1Cre; Arl13b*$^{lox/lox}$*; Ai9* (M) striatum. Arrowheads and arrow point to dynamic calcium hot spots in control cilia. Such hot spots are comparatively rare in Arl13b deficient cilia (N). Data shown are mean ± SEM. $^{*}P<0.05$ (Student's *t*-test, $p_{[N]}$ = 0.0005). Scale bar, 2μm (A, B, L, M); 1.4μm (D–G). See also Figure S4.

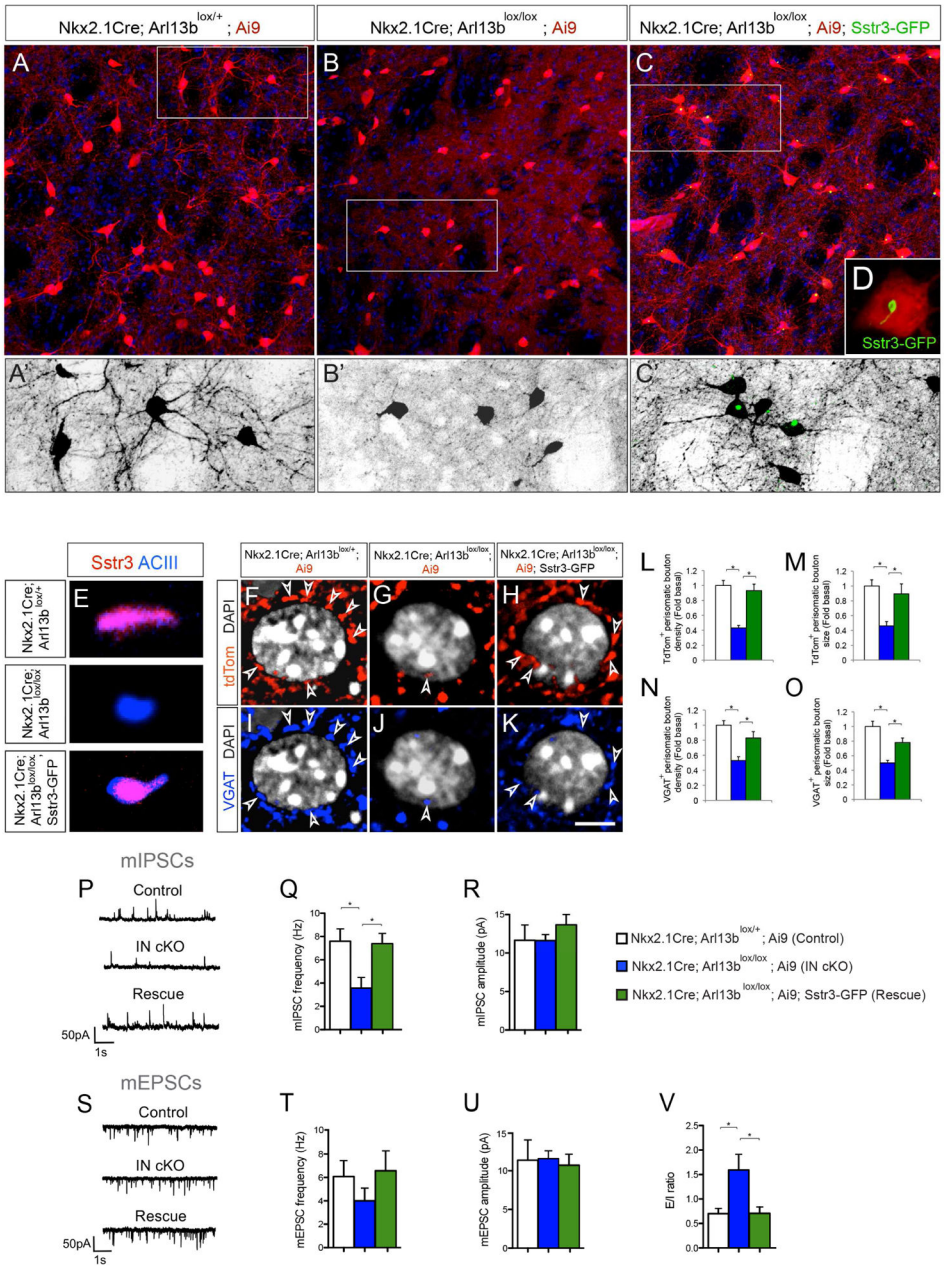

Figure 5. Primary cilia-driven Sstr3 signaling regulates interneuron morphology and connectivity

(A–C) Striatal tdTom^{+} INs in *Nkx2.1Cre; Arl13b$^{lox/+}$; Ai9* (A), *Nkx2.1Cre; Arl13b$^{lox/lox}$; Ai9* (B), and *Nkx2.1Cre; Arl13b$^{lox/lox}$; Ai9; Sstr3-GFP* (C) brains [P30]. (A′–C′) Higher-magnification images of tdTom^{+} striatal INs from outlined area in panels A–C. (D) Induced Sstr3-GFP expression in primary cilia of *Nkx2.1Cre; Arl13b$^{lox/lox}$; Sstr3-GFP; Ai9* INs. (E) Altered Sstr3 localization in Arl13b deficient IN primary cilia and re-expression after induction of Sstr3-GFP. Co-labeling of primary cilia with anti-ACIII and anti-Sstr3 antibodies in *Nkx2.1Cre; Arl13b$^{lox/+}$; Ai9*, *Nkx2.1Cre; Arl13b$^{lox/lox}$; Ai9* and *Nkx2.1Cre; Arl13b$^{lox/lox}$; Ai9^{+}; Sstr3-GFP* INs. (F–K) Perisomatic boutons (arrowheads) labeled with

tdTom (F–H) and anti-VGAT antibodies (I–K) in *Nkx2.1Cre; Arl13b$^{lox/+}$; Ai9* (F, I), *Nkx2.1Cre; Arl13b$^{lox/lox}$; Ai9* (G, J) and *Nkx2.1Cre; Arl13b$^{lox/lox}$; Sstr3-GFP; Ai9* (H, K) brains [P30]. (L–M) Quantification of tdTom^{+} perisomatic bouton density (L) and size (M). Data shown are mean ± SEM. $^{*}P<0.05$ (One-way ANOVA: $F_{2,42\ [L]} = 23.0$; p = 5.53616E-07; post-hoc $p_{[L,\ lox/+\ vs.\ lox/lox]}$ = 6.08809E-08, post-hoc $p_{[L,\ lox/lox\ vs.\ lox/lox\text{-}Sstr3]}$ = 3.26839E-05; $F_{2,42\ [M]} = 6.54$; p = 0.004; post-hoc $p_{[M,\ lox/+\ vs.\ lox/lox]}$ = 3.64284E-05, post-hoc $p_{[M,\ lox/lox\ vs.\ lox/lox\text{-}Sstr3]}$ = 0.008). n = 15 cells from 3 different brains per group. (N–O) Quantification of VGAT^{+} perisomatic bouton density (N) and size (O). Data shown are mean ± SEM. $^{*}P<0.05$ (One-way ANOVA: $F_{2,42\ [N]} = 13.35$; p = 5.6345E-05; post-hoc $p_{[N,\ lox/+\ vs.\ lox/lox]}$ = 5.21332E-06, post-hoc $p_{[N,\ lox/lox\ vs.\ lox/lox\text{-}Sstr3]}$ = 0.004; $F_{2,42\ [O]}$ = 17.68; p = 6.04031E-06; post-hoc $p_{[O,\ lox/+\ vs.\ lox/lox]}$ = 4.23172E-06, post-hoc $p_{[O,\ lox/lox\ vs.\ lox/lox\text{-}Sstr3]}$ = 0.0009). n = 15 cells from 3 different brains per group. (P–U) Patch-clamp electrophysiological recordings of striatal MSNs from *Nkx2.1Cre; Arl13b$^{lox/+}$; Ai9* (control, n=6), *Nkx2.1Cre; Arl13b$^{lox/lox}$; Ai9* (mutant, n=10) and *Nkx2.1Cre; Arl13b$^{lox/lox}$; Sstr3-GFP; Ai9* (rescue, n=4) brains. (P, S) Representative patch-clamp electrophysiological recordings from MSNs showing mIPSCs (P) and mEPSCs (S). (Q, R) Quantification of mIPSC frequency (Q) and amplitude (R). $^{*}P<0.05$ (One-way ANOVA, mIPSC frequency: $F_{2,20} = 7.7$; p = 0.003; post-hoc $p_{[ctrl\ vs.\ IN\ cKO]} < 0.01$, post-hoc $p_{[Rescue\ vs.\ IN\ cKO]} < 0.05$; control, n = 6; IN cKO, n = 11; rescue, n = 6). (T, U) Quantification of mEPSC frequency (T) and amplitude (U). (V) Rescue of overall excitatory/inhibitory ratio in striatal MSNs of *Nkx2.1Cre; Arl13b$^{lox/lox}$; Sstr3-GFP; Ai9* mice. Data shown are mean ± SEM. $^{*}P<0.05$ (One-way ANOVA: $F_{2,19} = 4.8$; p = 0.021; post-hoc $p_{[ctrl\ vs.\ IN\ cKO]} < 0.05$, $p_{[Rescue\ vs.\ IN\ cKO]} < 0.05$; control, n = 6; IN cKO, n = 10; rescue, n = 6). Scale bar, 37.6μm (A–C); 18μm (A′–C′); 6.2μm (D); 1.3μm (E); 5μm (F–K). See also Figure S5.

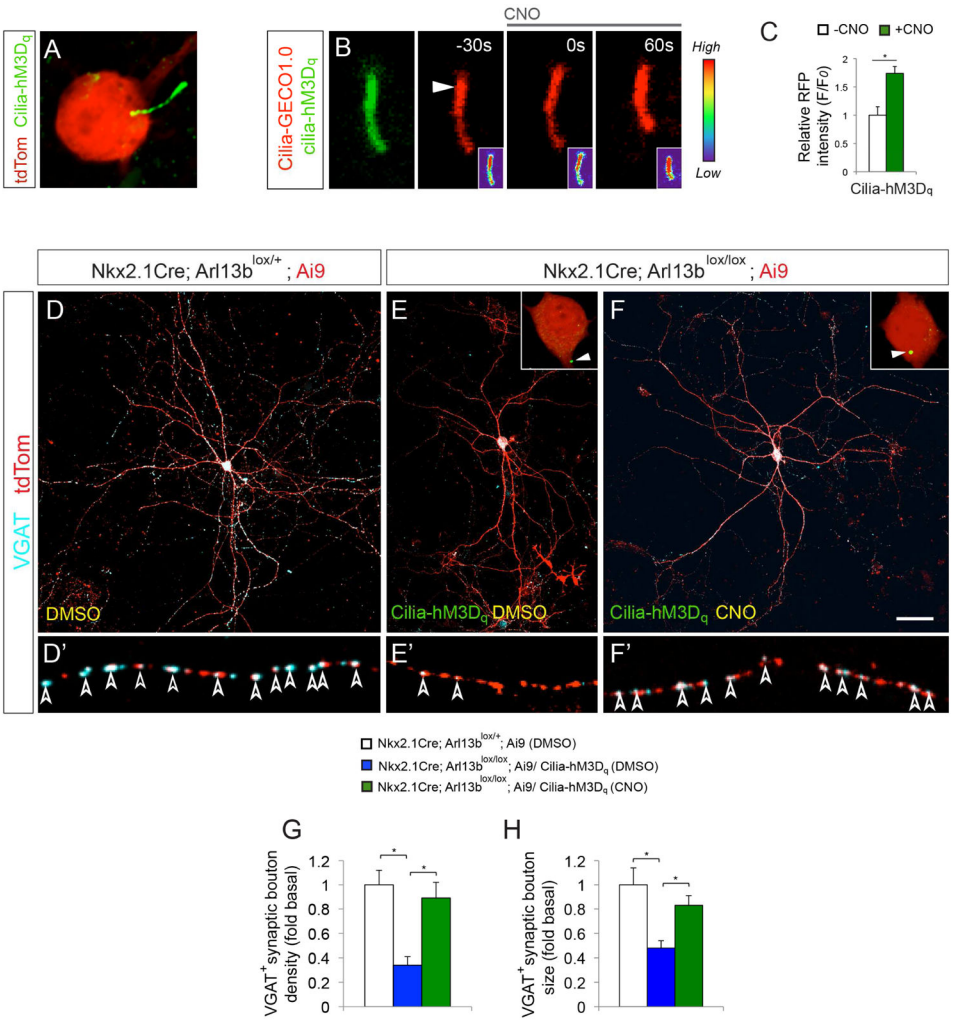

Figure 6. DREADD mediated chemogenetic activation of primary cilia-GPCR signaling rescues morphological and synaptic defects in Arl13b deficient interneurons

(A) Expression of Cilia-hM3D$_q$ in the primary cilia of tdTom$^+$ control interneurons. (B) Changes in ciliary Ca^{2+} dynamics upon CNO (10μM) exposure in control INs expressing Cilia-hM3D$_q$ (green) and Cilia-R-GECO1.0 (red). Arrowhead indicates cilia tip from where changes in fluorescence intensity were measured. Insets (B) show changes of fluorescence intensity in pseudocolor (Red [High], Blue [Low]). Time elapsed is indicated in seconds. (C) Quantification of changes in cilia-GECO1.0 intensity upon CNO treatment. Data shown are mean ± SEM. $^*P<0.05$ (Student's *t*-test, p = 0.0006). 15 cells from 3 independent experiments were analyzed per group. (D–F) Activation of ciliary GPCR signaling rescued Arl13b deficient phenotype. Anti-VGAT antibody labeled tdTom$^+$ INs from *Nkx2.1Cre; Arl13b$^{lox/+}$; Ai9* (D), and *Nkx2.1Cre; Arl13b$^{lox/lox}$; Ai9* mice expressing Cilia-hM3D$_q$ (E, F). INs in D–E and F were treated with DMSO and CNO, respectively. Insets (E, F) show high-magnification images of Cilia-hM3D$_q$ expression (arrowhead). (D′–F′) High-magnification images of axonal segments in D–F showing VGAT$^+$ synaptic boutons (arrowheads). (G, H) Quantification of VGAT$^+$ synaptic bouton density (I) and size (J) in tdTom$^+$ interneurons. Data shown are mean ± SEM. $^*P<0.05$ (One-way ANOVA: $F_{2,33[G]}$ =

15.92; $p_{[G]}$ = 1.44379E-05; post-hoc $p_{[G][lox/+ \text{ vs. } lox/lox (DMSO)]}$ = 5.46811E-06, $p_{[G][lox/lox (CNO) \text{ vs. } lox/lox (DMSO)]}$ = 0.0002; $F_{2,33[H]}$ = 13.07; $p_{[H]}$ = 6.59073E-05; post-hoc $p_{[H][lox/+ \text{ vs. } lox/lox (DMSO)]}$ = 8.88938E-05, $p_{[H][lox/lox (CNO) \text{ vs. } lox/lox (DMSO)]}$ = 0.001). 12 cells from 3 independent experiments were analyzed per group. Scale bar, 5.4μm (A); 2μm (B); 40μm (D–F); 7.8μm (D′–F′). See also Figure S6.

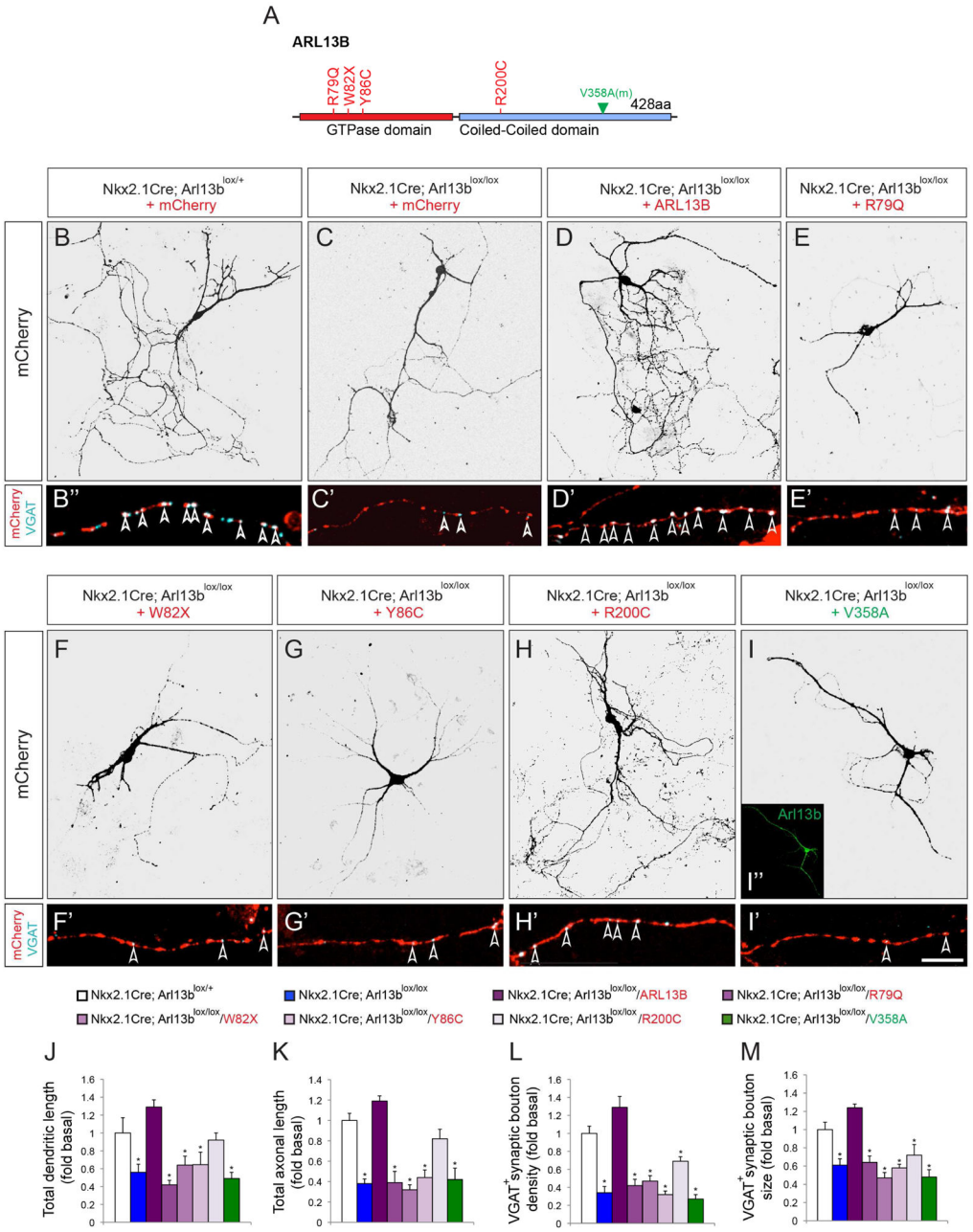

Figure 7. The effect of Jourbert-Sydrome linked human ARL13B alleles in Arl13b deficient interneurons

(A) Schematic of human ARL13B mutations and mouse non-cilia targeted Arl13b. (B–I) Dissociated INs from *Nkx2.1Cre; Arl13b*$^{lox/+}$*; Ai9* (B) or *Nkx2.1Cre; Arl13b*$^{lox/lox}$*; Ai9* (C–I) mice were transfected with AAV-mCherry (B, C), AAV-mCherry-ARL13B (D), R79Q (E), W82X (F), Y86C (G), R200C (H), and mV358A (I). Inset (I) shows non-ciliary expression of Arl13b^{V358A}. (B′–I′) Labeling with anti-VGAT antibodies show inhibitory presynaptic boutons (arrowhead) along mCherry^{+} IN axons (B–I). (J, K) Quantification of total dendritic (J) and axonal length (K). (L, M) Quantification of VGAT^{+} bouton density (L) and size (M) along axons. Data shown are mean ± SEM. 12 cells from 3 independent experiments were

analyzed per group. $^{*}P<0.05$ (One-way ANOVA: $F_{7,88}$ = 13.27[J], 17.61[K], 25.75[L], 23.52[M]; p = 1.43E-11[J], 2.11E-14[K], 8.13E-19[L], 1.06E-17[M]; post-hoc $p_{[lox/+ \text{ vs. } lox/lox}$ = 0.001[J], 7.50E-08[K], 2.34E-06[L], 0.0003[M]; post-hoc $p_{[lox/+ \text{ vs. } lox/lox\text{-}ARL13B}$ = 0.06[J], 0.1[K], 0.08[L], 0.09[M]; post-hoc $p_{[lox/+ \text{ vs. } lox/lox\text{-}R79Q]}$ = 9.38E-06 [J], 6.50E-05[K], 6.44E-06[L], 0.0003[M]; post-hoc $p_{[lox/+ \text{ vs. } lox/lox\text{-}W82X]}$ = 0.009 [J], 3.51E-08[K], 1.15E-05[L], 2.14E-06[M]; post-hoc $p_{[lox/+ \text{ vs. } lox/lox\text{-}Y86C]}$ = 0.002 [J], 6.42E-06[K], 7.67E-08[L], 9.10E-06[M]; post-hoc $p_{[lox/+ \text{ vs. } lox/lox\text{-}R200C]}$ = 0.46[J], 0.06[K], 0.002[L], 0.004[M]; post-hoc $p_{[lox/+ \text{ vs. } lox/lox\text{-}V358A]}$ = 0.0001[J], 6.91E-05[K], 5.2771E-08[L], 1.63E-05[M]. Scale bar, 40μm (B–I); 10μm (B′–I′).